

Multimode Fock states with large photon number: effective descriptions and applications in quantum metrology

M. Perarnau-Llobet,^{1,2,*} A. González-Tudela,³ and J. I. Cirac^{1,2}

¹Max-Planck-Institut für Quantenoptik, Hans-Kopfermann-Str. 1, D-85748 Garching, Germany

²Munich Center for Quantum Science and Technology (MCQST), Schellingstr. 4, D-80799 München

³Instituto de Física Fundamental IFF-CSIC, Calle Serrano 113b, Madrid 28006, Spain.

(Dated: February 20, 2022)

We develop general tools to characterise and efficiently compute relevant observables of multimode N -photon states generated in non-linear decays in one-dimensional waveguides. We then consider optical interferometry in a Mach-Zender interferometer where a d -mode photonic state enters in each arm of the interferometer. We derive a simple expression for the Quantum Fisher Information in terms of the average photon number in each mode, and show that it can be saturated by number-resolved photon measurements that do not distinguish between the different d modes.

I. INTRODUCTION

Photonic states with a large and fixed number N of photons play a crucial role in quantum technologies but are extremely challenging to prepare experimentally. The paradigmatic example are single-mode Fock states, $|N\rangle \propto (a^\dagger)^N|0\rangle$, where all the photons share the same spatio-temporal mode (a^\dagger), and which are the basis of many quantum metrology protocols [1–4]. Nowadays, the most widely used method to generate them is based on combining with post-selection heralded single photons emitted in spontaneous parametric down-conversion processes [5–9]. This method, however, suffers from an exponential decrease of efficiency with N , hindering its application for large photon numbers. Single-mode Fock states can also be emitted naturally from entangled atomic states in ensembles with many more atoms than N [10]. However, exciting such atomic states is highly non-trivial because of the linear energy spectrum of such systems [11–14].

A way of circumventing these limitations is the use non-linear systems for the generation of such photonic states. These type of systems appear in many different contexts, such as in cavities with Kerr-type non-linearities [15], in multi-level quantum dots due to biexciton binding-energies [16, 17], or even in atomic ensembles simply because an atom can not be doubly excited or by exploiting Rydberg blockade [18, 19]. These mechanisms ultimately translate into either non-harmonic energy splittings (Kerr cavity QED) or non-harmonic decay rates (saturation), which can be harnessed for multiphoton emission. An illustration of that is the proposal put forward by us in Ref. [20] to generate multiphoton states with quantum emitters coupled to photonic waveguides [21–30]. There, N excited emitters interact with the waveguide in the so-called mirror configuration [28, 31], such that its dynamics is described by the well-known Dicke model [32]. In that situation, the emitters experience a non-linear decay process, known as superradiant decay, which enhances the probability of emitting the photons into the waveguide as compared to other decay channels. Beyond the collective enhancement, the non-linearity has another effect: the

photons released into the waveguide have an inherent *multi-mode* structure [13]:

$$|\phi_A^{(N)}\rangle = \int \dots \int \frac{dk_1 \dots dk_N}{(2\pi)^N N!} A_{\{k\}} a_{k_1}^\dagger \dots a_{k_N}^\dagger |0\rangle, \quad (1)$$

where $a_{k_i}^\dagger$ is the creation operator of a waveguide photon of momentum k_i . The coefficient $A_{\{k\}} = A_{k_1, k_2, \dots, k_N}$ characterizes the multimodal structure of the wavepacket, and will be non-factorizable ($A_{\{k\}} \neq \sqrt{N!} A_{k_1} \dots A_{k_N}$) for photons emitted from any type of non-linear system (e.g., non-harmonic energies or non-linear decay rates). This non-trivial multimode nature of the emitted wavepackets forces one to revisit the results derived for single-mode Fock states as they are not necessarily valid anymore. For example, the multimodal structure poses limits on the scalability as Fock state sources from spontaneous parametric down conversion processes [33–35], is required to accurately predict the scattering of quantum pulses [36, 37], or, as we showed in our recent manuscript [20], renormalizes the results of single-mode quantum metrology protocols.

Motivated by these observations, the goal of this article is to develop general tools to deal with multimode states generated in non-linear decays, both from the point of view of its characterisation as well as applications in quantum metrology. We start by considering a general N -dimensional emitter decaying in a non-linear fashion with a waveguide. The wavefunction of the emitted photonic state (given by $A_{\{k\}}$ in (1)) can be obtained through the techniques of [38], and it involves $N!$ terms due to bosonic symmetrisation. Given this highly non-trivial state, the main contributions of this article are:

1. To develop a framework to compute relevant observables of multimode states generated in non-linear decays in an efficient manner, with the complexity scaling polynomially with N .
2. To apply these general tools to the characterisation of Dicke superradiant photonic states where we find that most photons are contained in a few modes: a single mode contains 91% of the photons, and two (three) modes already contain 98.4% (99.6%) of them.

Having identified general properties of multimode states, and in particular superradiant Dicke states, we then study their po-

* marti.perarnau@mpq.mpg.de

tential for quantum metrology [1–4]. Building on our previous work [20], our goal is to extend well known results in quantum optical interferometry [39, 40] to the presence of a non-trivial multimode structure within the input photonic states, as in Eq. (1). For that, we consider phase estimation in a Mach-Zender interferometer, where the input state of each arm of the interferometer is a generic d -mode state with a fixed total photon number. Then, our main contributions are:

1. We show that the quantum Fisher information [41] (QFI) \mathcal{Q} takes the particularly simple form

$$\mathcal{Q} = 2 \sum_{j=1}^d n_j(m_j + 1) + m_j(n_j + 1). \quad (2)$$

where n_i, m_i are the average photon number in the i th mode of the two incoming wavepackets.

2. We show that the QFI (2) can be saturated by number-resolved measurements which *cannot* distinguish between the different d modes.
3. Finally, we also discuss the effect of photon loss in the interferometer and in the measurement devices given the proposal of [20] for quantum-enhanced metrology with twin Dicke superradiant states.

The paper is structured as follows: We start presenting the general multimode structure of the photons emitted from non-linear systems into waveguides in Section III, whereas the tools to characterize such photonic states are developed in Section III. These tools are applied to superradiant photonic states in Section IV. In Section V we consider quantum metrology with multimode states, and finally we summarize our findings in Section VI.

II. NON-LINEAR SYSTEMS DECAYING IN 1D WAVEGUIDES

In the interest of generality, we consider the emission process coming from a N -level system ($|0\rangle, |1\rangle, \dots, |N\rangle$) with energies ω_j . Its free Hamiltonian is then given by (taking $\hbar \equiv 1$):

$$H_S = \sum_{j=1}^N \omega_j \sigma_{j,j} \quad (3)$$

with $\sigma_{ik} = |i\rangle\langle k|$. The system is coupled to a 1D waveguide, described by a one-dimensional and chiral photon bath with a linear dispersion (both the chirality and linearity assumptions can be relaxed obtaining similar results) $\omega_q = cq$. Taking $c \equiv 1$, its Hamiltonian read:

$$H_B = \int dq q a_q^\dagger a_q. \quad (4)$$

Finally, the system-bath interaction Hamiltonian is assumed to be given by:

$$H_{SB} = \sum_{j=1}^N \sqrt{\gamma_j} \int \frac{dq}{2\pi} (a_q^\dagger \sigma_{j-1,j} + a_q \sigma_{j,j-1}). \quad (5)$$

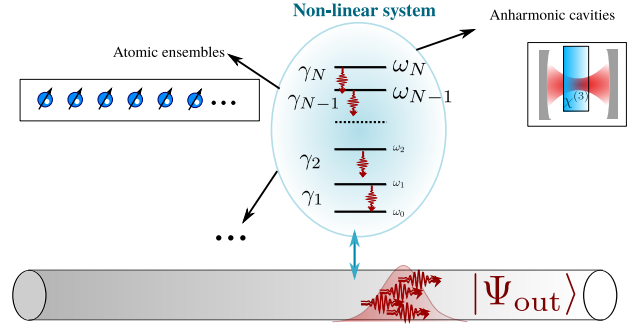


FIG. 1. A the non-linear system (in blue) with N levels with energy ω_n , couples to a 1D waveguide. The coupling with the waveguide induce single-photon transitions $n \rightarrow n - 1$ (in red arrows) at a rate γ_n . Around the non-linear system, we depict the two example of non-linear system that we consider along the manuscript, that are, equally spaced atomic ensembles and anharmonic cavities.

where γ_j denotes the decay rate of the transition from the j -th to the $(j - 1)$ -th level. The global Hamiltonian describing the emission process is then given by the sum of the three terms: $H = H_S + H_B + H_{SB}$. The whole physical set-up is illustrated in Figure 1.

We consider that initially the waveguide B is in the ground state, whereas the system S initially contains N excitations. When the excitations decay into the waveguide, the photonic state is described by the wavefunction (naturally extending the considerations of [13]):

$$|\phi^{(N)}\rangle = \frac{1}{N!} \int \dots \int_0^\infty A_{t_1 \dots t_N} \prod_{j=1}^N dt_j a_{t_j}^\dagger |0\rangle \quad (6)$$

with

$$A_{t_1 \dots t_N} = \mathcal{T}(\langle \varphi_0 | \mathcal{O}_{t_1} \dots \mathcal{O}_{t_N} | \varphi_N \rangle) \quad (7)$$

where \mathcal{T} stands for time-ordering, and \mathcal{O}_t satisfies $\langle \varphi_{j-1} | \mathcal{O}_t = \sqrt{\gamma_j} e^{[i(\omega_{j-1} - \omega_j) + \frac{1}{2}(\gamma_{j-1} - \gamma_j)]t} \langle \varphi_j |$. Furthermore, the bosonic creation and annihilation operators a_s, a_s^\dagger satisfy the standard commutation relation

$$[a_s, a_t^\dagger] = \delta(s - t). \quad (8)$$

The use of this general light-matter Hamiltonian H allows to capture the physics of very different models, such as:

- *Saturated atomic ensembles in the atomic mirror configuration.* As explained in Refs. [13, 20], within the Markov approximation the coupling of the ensemble with the waveguide can be described by a single collective dipole operator. This can be effectively described as N -level system with equally spaced energy levels, $\omega_n = n\omega_0$, but non-linear decay rates: $\gamma_n = \Gamma_{1d} n(N - n + 1)$. In the text, we shall call these emitted states *superradiant states*, or *superradiant photonic states*.

- *Anharmonic cavities.* In the case of a non-linear resonator, with a Kerr non-linearity of the form $H_B = \omega_a a^\dagger a + U a^\dagger a (a^\dagger a - 1)$, but coupled to the waveguide in a linear fashion such that its reduced dynamics is given by the standard Lindblad form $\Gamma_{1d}(2apa^\dagger - a^\dagger a \rho - \rho a^\dagger a)/2$, the energy levels are now non-linear: $\omega_n = n\omega_a + n(n-1)U$, while the decay rates are harmonic $\gamma_n = n\Gamma_{1d}$.

Along this manuscript, we will focus on the characterization of the first ones, as they will be the most relevant for quantum metrology. However, all the formalism developed is valid for any combination of $\{\omega_n, \gamma_n\}$.

III. TOWARDS EFFECTIVE CHARACTERISATIONS OF MULTIMODE STATES

We start this section by developing techniques that enable us to compute relevant observables of $|\phi^{(N)}\rangle$ efficiently for large N . This is motivated by noting that the analytical form (6) contains $N!$ terms due to the time ordering in (7), making such an expression challenging to handle beyond low N .

We first consider a single emitted photon (with $\gamma \equiv \gamma_1 - \gamma_0$ and $\omega \equiv \omega_1 - \omega_0$):

$$|\phi^{(1)}\rangle = \int_0^\infty dt B_t^{(\gamma, \omega)} a_t^\dagger |0\rangle \equiv b_{\gamma, \omega}^\dagger |0\rangle \quad (9)$$

where we have defined $B_t^{(\gamma, \omega)} \equiv \sqrt{\gamma} e^{-t(i\omega + \frac{\gamma}{2})}$ and $b_{\gamma, \omega}^\dagger \equiv \int_0^\infty dt B_t^{(\gamma, \omega)} a_t^\dagger$. Using (8), the commutation relation

$$[b_{\gamma, \omega}, b_{\gamma', \omega'}^\dagger] = \frac{2\sqrt{\gamma\gamma'}}{\gamma + \gamma' + 2i(\omega' - \omega)} \quad (10)$$

follows. Given such single-mode operators $b_{\gamma, \omega}$'s, we have developed techniques to compute efficiently observables of the form

$$\langle \phi^{(N)} | b_{x_1, y_1} \dots b_{x_n, y_n} b_{\tilde{x}_1, \tilde{y}_1}^\dagger \dots b_{\tilde{x}_n, \tilde{y}_n}^\dagger | \phi^{(N)} \rangle. \quad (11)$$

The computational techniques for dealing with (11) are rather involved and are developed in detail in the Appendix I. Here, we instead explain the main ideas and implications:

1. The computation of (11) is developed by expressing it as a recurrence relation, which is then transformed into a matrix multiplication.
2. The solution is exact as the integrals in (6) are carried out analytically. Yet, in practice it is convenient to perform the matrix multiplication numerically in order to access large N .
3. The size of the involved matrices is at most $(4^n(N - n + 1))^2$, although usually this can be reduced if there are some symmetries in the calculation (i.e. if some of the x_i 's and y_i 's in (11) are the same). In practice, this means that for $n = 1$ (corresponding to average photon number), one can easily reach up to $N \approx 1000$,

whereas for $n = 2$ (corresponding to the variance) one can reach $N \approx 100$. This should be contrasted to the naive calculation of (11) from (6) which involves $(N!)^2$ integrals.

4. Since the $b_{\gamma, \omega}^\dagger$'s form an (overcomplete) basis of the Fock space spanned by $a_t^\dagger \forall t$, one can in principle compute arbitrary observables through this approach.

IV. CHARACTERISATION OF SUPERRADIANT PHOTONIC STATES

We now apply the machinery developed in the previous section to the characterisation of superradiant photonic states emitted when N excited atoms are placed next to the waveguide in the atomic mirror configuration, as previously proposed by us in [20]. This corresponds to taking $|\phi^{(N)}\rangle$ in (11) with $\gamma_n = \Gamma_{1d}n(N - n + 1)$ and $\omega_n = n\omega_0$.

Before proceeding to its characterisation, let us mention that there are two main features that make this proposal particularly appealing [20]:

- In the absence of photon loss (i.e., when the atom-waveguide set-up is perfectly isolated) and assuming perfect control on the system's Hamiltonian, the protocol is *deterministic* and *scalable*. That is, simply by placing more atoms next to the waveguide, one can generate a larger N -photon state.
- In the presence of photon loss in free space, the probability of success scales as $\approx 1 - \ln(N)(\Gamma^*/\Gamma_{1d})$, where Γ_{1d} is the decay rate into the waveguide and Γ^* into free space, for $\Gamma^*/\Gamma_{1d} \ll 1$. This slow decrease with $\ln N$ arises due to the enhanced collective decay and should be contrasted with the standard success probability $\approx 1 - N(\Gamma^*/\Gamma_{1d})$ obtained for N independent decay processes (see Ref. [20] for more details).

Hence, Dicke superradiant decays provide a natural framework to generate N -photon states in a deterministic, scalable and robust-to-photon-loss manner. Furthermore, current experimental nanophotonic platforms have already achieved ratios $\Gamma_{1d}/\Gamma^* \approx 60$ with $\Gamma_{1d} \sim 1$ GHz [26].

A. Average photon number

We first consider the photon number

$$n(\gamma, \omega) \equiv \langle \phi^{(N)} | b_{\gamma, \omega}^\dagger b_{\gamma, \omega} | \phi^{(N)} \rangle. \quad (12)$$

We start by fixing the decay rate γ and varying ω around ω_0 , corresponding to the frequency of the two-level emitters. Figure 2 shows how the average photon number is centred at ω_0 , as one would have expected physically.

Next we consider $n(\gamma, \omega)$ for a fixed $\omega = \omega_0$ and varying γ . The results are shown in Fig. 3, where we compute $n(\gamma, \omega_0)$ for $N = 100, 200, 300$. Interestingly, note that the maximum of $n(\gamma, \omega)$ appears at $x = N/\ln N$. To understand

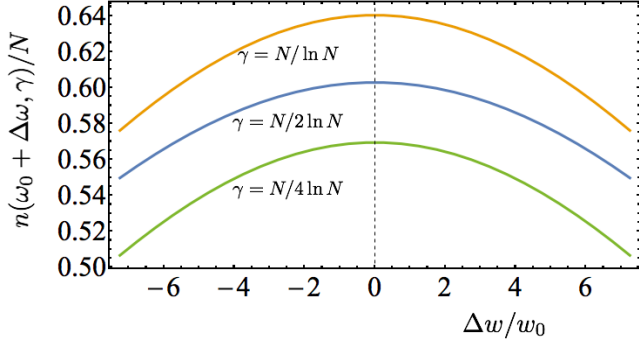


FIG. 2. Ratio of photons of a superradiant N -photon state $|\phi^{(N)}\rangle$ in a mode with frequency $\omega_0 + \Delta\omega$ and inverse decay rate γ .

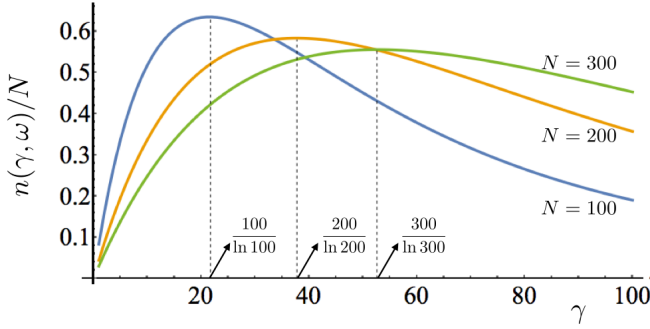


FIG. 3. Ratio of photons of a superradiant N -photon state $|\phi^{(N)}\rangle$ in a mode with frequency ω_0 and varying inverse decay rate γ . Note that the maximal number of photons is found for $\gamma \approx N/\ln N$.

this, note that the time scale τ of decay of the photons is proportional to γ^{-1} . In particular, for the superradiant decay, the j th collective excitation decays with a time scale γ_j^{-1} , with $\gamma_j = \Gamma j(N - j + 1)$, and the average decay time is given by

$$\langle \tau \rangle \propto \sum_{j=1}^N \gamma_j^{-1} = \Gamma^{-1} \sum_{j=1}^N \frac{1}{j(N - j + 1)} \approx \Gamma^{-1} \frac{N}{2 \ln N}. \quad (13)$$

Hence, we realise from (6) that the choice $\gamma = N/\ln N$ corresponds to single-mode photons decaying with the average decay time of the superradiant photons. This provides an heuristic explanation for the optimal choice of γ that maximises $n(\gamma, \omega_0)$, i.e., the number of photons in the mode $b_{\gamma, \omega}$.

B. Most relevant modes

The results of Figures 3 and 2 suggest that a rather large proportions of photons (between 50% and 60% for $N = 100, 200, 300$) can be contained in a small set of modes centred around the frequency ω and with inverse decay rate $\gamma = N/\ln N$. This motivates us to consider a set of D modes with frequency ω_0 and varying $\Gamma = jN/\ln N$, with $j = 1, \dots, D$; that is, $\{b_{jx, \omega_0}\}_{j=1}^D$ with $x = N/\ln N$. Note that these modes

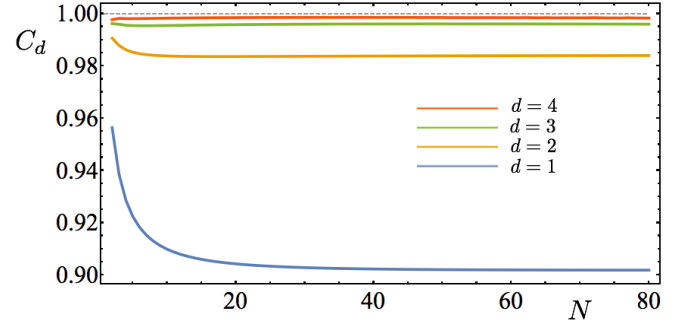


FIG. 4. Proportion of photons in d modes as quantified by (19) for $D = 10$ as a function of the number of photons N in the superradiant state.

are not orthogonal due to (10). A set of orthogonal modes can be constructed by solving the generalised eigenvalue equation,

$$T \vec{v}^{(k)} = \lambda_k R \vec{v}^{(k)} \quad (14)$$

where T and R are matrices of size D^2 whose elements are given by

$$T_{kl} = \langle \phi^{(N)} | b_{kx, \omega_0}^\dagger b_{lx, \omega_0} | \phi^{(N)} \rangle, \quad R_{kl} = [b_{kx, \omega_0}, b_{lx, \omega_0}^\dagger] = \frac{2\sqrt{kl}}{k+l}. \quad (15)$$

This leads to a set of D bosonic modes

$$c_k = \sum_{j=1}^D v_j^{(k)} b_{jx, \omega_0} \quad \text{with} \quad x = \frac{\ln N}{N}, \quad (16)$$

The usual commutation relations

$$[c_i, c_j^\dagger] = \delta_{ij}, \quad (17)$$

are guaranteed by (14) (plus appropriate normalisation).

Let us now define the number operators (for a given D),

$$n_d \equiv \sum_{j=1}^d c_j^\dagger c_j, \quad (18)$$

and the corresponding ratio of photons,

$$C_d = \frac{\langle \phi^{(N)} | n_d | \phi^{(N)} \rangle}{N}. \quad (19)$$

In Figure 4, we show C_d as a function of N for $D = 10$ (i.e. the modes c_k 's are a linear combination of 10 modes b_{kx, ω_0} 's). Note that C_d quickly saturates with N . The values of C_d for different D 's are shown in the following Table, which is evaluated at $N = 100$:

	C_1	C_2	C_3	C_4	C_5	C_6	C_7	C_8
D=2	0.653	0.688						
D=4	0.852	0.918	0.921	0.921				
D=6	0.894	0.973	0.980	0.981	0.981	0.981		
D=8	0.901	0.983	0.993	0.995	0.995	0.995	0.995	0.995
D=10	0.902	0.984	0.996	0.998	0.999	0.999	0.999	0.999

These numbers can be slightly increased by considering larger d 's or D 's. It is remarkable that with only 2 (3) modes we can cover 98.4% (99.6%) of the photons, and that more than 90% photons live in a single mode. Hence, although the superradiant state $|\phi^{(N)}\rangle$ may naively appear as a highly multimode state, it can be described by means of only a few modes. At the same time, it is worth noticing that although we reached this result by a rather heuristic method, these descriptions are almost optimal: since the small set of considered modes already contains around 99.9% of the photons, it is not possible that by considering a much larger (possibly infinite) set of modes the effective descriptions can considerably change. In other words, while a few modes seem to suffice to describe $|\phi^{(N)}\rangle$ with high accuracy, it is not possible to describe it by a single one.

C. Variance

Let us further characterise the fact that most photons are contained in a few modes by studying the fluctuations of the number operators n_k 's given in (18). In particular consider the variance

$$\sigma_{n_d} = \sqrt{\langle n_d^2 \rangle - (\langle n_d \rangle)^2}, \quad (20)$$

with $\langle \dots \rangle \equiv \langle \phi^{(N)} | \dots | \phi^{(N)} \rangle$. To compute such expressions, first we expand them using the commutation relations (17) as

$$\begin{aligned} \langle n_1^2 \rangle &= \langle c_1^2 (c_1^\dagger)^2 \rangle - 3\langle n_1 \rangle - 2 - (\langle n_1 \rangle)^2 \\ \langle n_2^2 \rangle &= \langle c_1^2 (c_1^\dagger)^2 \rangle + \langle c_2^2 (c_2^\dagger)^2 \rangle + 2\langle c_1 c_2 c_1^\dagger c_2^\dagger \rangle \\ &\quad - 5\langle n_1 \rangle - 5\langle n_2 \rangle - 6 \end{aligned} \quad (21)$$

and similarly for higher $\langle n_j^2 \rangle$. Each term can be evaluated by using (16) and then computing $\langle b_i b_j b_k^\dagger b_l^\dagger \rangle$ (or $\langle b_i b_j \rangle$) by the appropriate recurrence relation derived in Appendix I. For numerical purposes, it is convenient to first compute $\langle b_i b_j b_k^\dagger b_l^\dagger \rangle \forall i, j, k, l$ where $i = 1, \dots, D$ and save the results. In the numerical simulations of this section, we take $D = 8$, for which we already cover 99% of the photons as shown in Table IV B. The results are shown in Figure 5 for $d = 1, 2, 3$ and $D = 8$. As expected, σ_{n_d} decreases as d increases, and for $d = 3$ and $D = 8$ the variance is rather small: less than one photon for $N = 40$. This confirms the previous results that a few modes can cover most of the photons contained in the superradiant state. Furthermore, we also observe that σ_{n_d} grows linearly with N , which is compatible with the proportion of photons staying constant with N as shown in Figure 2.

D. Effective descriptions

The main insight of the previous sections is that 2 or 3 modes suffice to describe most of the photons of $|\phi^{(N)}\rangle$. We can use this insight to build effective descriptions of $|\phi^{(N)}\rangle$ within these subspaces. This can be achieved by computing

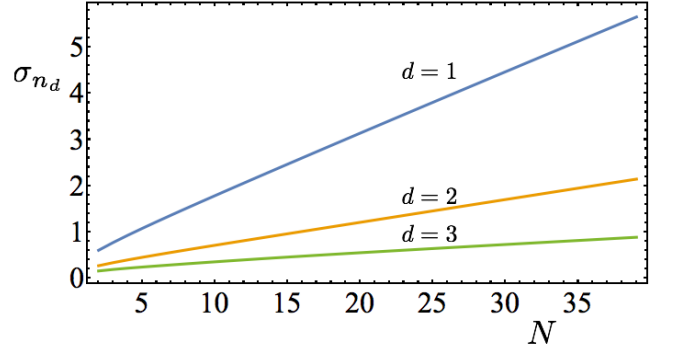


FIG. 5. Variance of the number operators n_1, n_2 , and n_3 defined in (18) for $D = 8$.

the overlaps

$$\langle 0 | c_1^{k_1} c_2^{k_2} \dots c_d^{k_d} | \phi^{(N)} \rangle, \quad (22)$$

for all $\{c_j\}_{j=1}^d$ such that $\sum_d k_d = N$, and where d is the number of considered modes. For that, we first express (22) as a combination of $\langle 0 | b_{x,\omega_0}^{k_1} b_{2x,\omega_0}^{k_2} \dots b_{Dx,\omega_0}^{k_D} | \phi^{(N)} \rangle$ through (16). Then, in Appendix I, we develop a recurrence relation method to compute $\langle 0 | b_{x,\omega_0}^{k_1} b_{2x,\omega_0}^{k_2} \dots b_{Dx,\omega_0}^{k_D} | \phi^{(N)} \rangle$ which requires the multiplication of $\mathcal{O}(N)$ matrices of dimension \dim , which satisfies $N \lesssim \dim \lesssim (N/D)^D$. In order to compute (22), it is convenient to first compute all possible $\langle 0 | b_{x,\omega_0}^{k_1} b_{2x,\omega_0}^{k_2} \dots b_{Dx,\omega_0}^{k_D} | \phi^{(N)} \rangle$ for all $\{k_j\}_{j=1}^N$ such that $\sum_j k_j = N$ and save such coefficients. There are $\mathcal{O}(N^D)$ such coefficients, which provides the necessary space to carry out the computation. Overall, the whole computation is challenging, both in terms of the number of operations and the complexity of each one, but becomes feasible for small N and $D \leq 10$, which is enough to capture most of the photons (see Table IV B).

We consider the following unnormalised two and three mode state:

$$\begin{aligned} |\psi_2^{(N)}\rangle &= \sum_{j=0}^N \alpha_j |j, N-j\rangle \\ |\psi_3^{(N)}\rangle &= \sum_{j=0}^N \sum_{k=0}^{N-j} \alpha_{j,k} |j, k, N-j-k\rangle \end{aligned} \quad (23)$$

with $|j, N-j\rangle = (c_1^\dagger)^{N-j} (c_2^\dagger)^j |0\rangle / \sqrt{(N-j)!j!}$, $|j, k, N-j-k\rangle = (c_1^\dagger)^j (c_2^\dagger)^k (c_3^\dagger)^{N-j-k} |0\rangle / \sqrt{(N-j-k)!k!j!}$, $\alpha_j = \langle \phi^{(N)} | j, N-j \rangle$ and $\alpha_{j,k} = \langle \phi^{(N)} | j, k, N-j-k \rangle$. The normalisation (for two modes)

$$\mathcal{N} = \sum_{j=0}^N |\alpha_j|^2, \quad (24)$$

or $\mathcal{N} = \sum_{j,k} |\alpha_{j,k}|^2$ for three, indicates the overlap between $|\psi_{2,3}^{(N)}\rangle$ and $|\phi^{(N)}\rangle$, i.e., how good the approximation in the

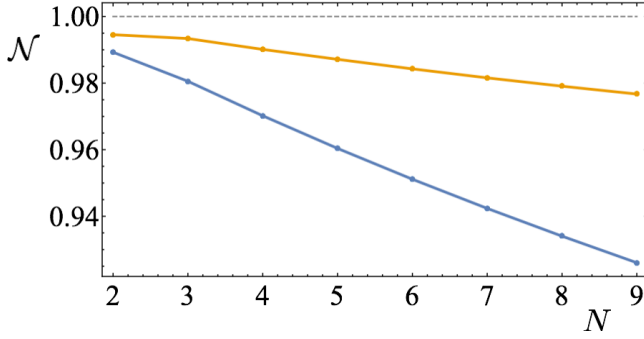


FIG. 6. Overlap for the two-mode (blue) and three-mode (orange) approximations for $D = 8$.

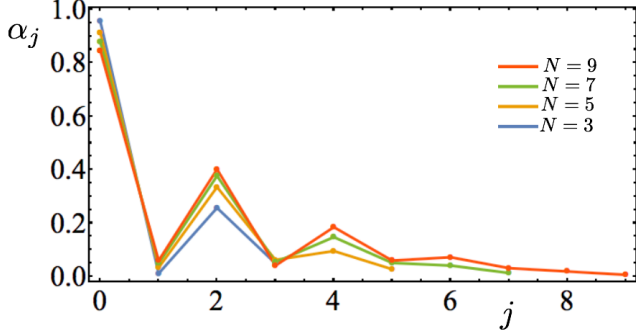


FIG. 7. Coefficients of the two-mode state for $N = 3, 5, 7, 9$ and $D = 8$.

two or three mode subspace is. In Figure 6, we show how \mathcal{N} is close to 1 for low $N \leq 10$, especially for $d = 3$ where it stays above 0.97. This implies that $|\phi^{(N)}\rangle$ can indeed be well described by two or three mode states as in (23). For $d = 2$, the coefficients are given in Figure 7 and the coefficients for $d = 3$ are provided in Appendix I. These approximate states of the form (23) become handy in calculations for quantum information tasks, as we will later illustrate for quantum metrology, and importantly our techniques enable us to quantify how close are our approximate states to the real $|\phi^{(N)}\rangle$. As a final remark, we note that the linear decrease of \mathcal{N} with N is also compatible with our previous results where we observed that the proportion of photons in a given mode stays constant.

V. APPLICATIONS IN QUANTUM METROLOGY

We now apply the different insights and techniques developed in the last section to quantum optical interferometry, in particular by considering phase estimation in a standard Mach-Zender (MZ) interferometer. We consider that each arm of the MZ interferometer is described by a set of modes $\{a_k\}_{k=1}^d$ and $\{b_k\}_{k=1}^d$, respectively (see Figure 8). When $d = 1$, we recover the standard two-mode optical interferometry [4], and our goal is precisely to extend well-known results to the multimode regime where $d > 1$. We start this section by introducing some basic concepts of quantum metrology, as

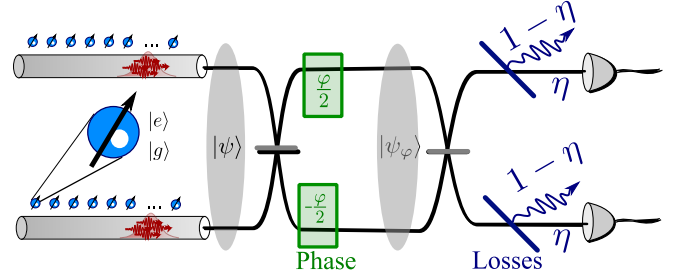


FIG. 8. A multimode state (generated e.g. through a superradiant decay) enters each arm of a MZ interferometer. Each arm of the interferometer is described by the set of modes: $\{a_k\}, \{b_k\}$.

well as describing the set-up we consider here in detail.

We consider the estimation of a parameter φ by measuring N photons which encode information about it. The (possibly entangled) N -photon state is described by $|\psi_\varphi\rangle$. Let us assume that we apply a measurement M on $|\psi_\varphi\rangle$, the statistics being described by a probability distribution $P(s_j|\varphi)$ where $\{s_j\}$ are the possible outcomes of the measurement given the value φ of the unknown parameter to be estimated. If this process is repeated ν times, in the limit $\nu \gg 1$ the Cramer-Rao bound guarantees that the mean-squared error $\Delta^2 \tilde{\varphi}$ of any unbiased and consistent estimator $\tilde{\varphi}$ of φ is lower bounded by [42, 43]:

$$\Delta^2 \tilde{\varphi} \geq \frac{1}{\nu \mathcal{C}} \quad (25)$$

where \mathcal{C} is the classical Fisher Information (CFI),

$$\mathcal{C} = \sum_j \frac{1}{P(s_j|\varphi)} \left(\frac{\partial P(s_j|\varphi)}{\partial \varphi} \right)^2. \quad (26)$$

The CFI quantifies the best resolution of a particular estimation scheme as defined through $|\psi_\varphi\rangle$ and a measurement M . In their seminal work, Braunstein and Caves optimised \mathcal{C} over all possible quantum measurements M [41]. The resulting quantity is the Quantum Fisher Information \mathcal{Q} (QFI), which satisfies,

$$\Delta^2 \tilde{\varphi} \geq \frac{1}{\nu \mathcal{C}} \geq \frac{1}{\nu \mathcal{Q}} \quad (27)$$

and, for pure states, is given by

$$\mathcal{Q} = 4 \left(\langle \dot{\psi}_\varphi | \dot{\psi}_\varphi \rangle - |\langle \dot{\psi}_\varphi | \psi_\varphi \rangle|^2 \right) \quad (28)$$

with $\dot{\psi}_\varphi = \partial_\varphi \psi_\varphi$. The QFI quantifies the potential of a particular state $|\psi_\varphi\rangle$ for quantum metrology [41].

Let us now discuss how we encode φ in the standard Mach-Zender (MZ) interferometer, but extended to the multimode regime. We consider as an initial state $|\psi\rangle = |\phi_A, \phi_B\rangle$, where

$$\begin{aligned} |\phi_A\rangle &= \sum_{\{\alpha_i\}_{i=1}^d \in \mathcal{C}(n)} C_{\{\alpha\}}^{(A)} |\{\alpha\}\rangle_a \\ |\phi_B\rangle &= \sum_{\{\alpha_i\}_{i=1}^d \in \mathcal{C}(m)} C_{\{\alpha\}}^{(B)} |\{\alpha\}\rangle_b \end{aligned} \quad (29)$$

with

$$\begin{aligned} |\{\alpha\}\rangle_a &= \frac{(a_1^\dagger)^{\alpha_1}}{\sqrt{\alpha_1!}} \dots \frac{(a_d^\dagger)^{\alpha_d}}{\sqrt{\alpha_d!}} |0\rangle \\ |\{\alpha\}\rangle_b &= \frac{(b_1^\dagger)^{\alpha_1}}{\sqrt{\alpha_1!}} \dots \frac{(b_d^\dagger)^{\alpha_d}}{\sqrt{\alpha_d!}} |0\rangle, \end{aligned} \quad (30)$$

and where $\{\alpha_i\} \in \mathcal{C}(n)$ iff $\sum_i \alpha_i = n$, and with $n + m = N$. That is, we consider that two independent (but generic) states of m and n photons, each of them described by d modes, enter the two arms of the interferometer. For $d = 1$, the states are single-mode states and hence Fock states. We also assume bosonic commutation relations,

$$[a_i, a_j^\dagger] = \delta_{ij}, \quad [b_i, b_j^\dagger] = \delta_{ij}, \quad (31)$$

which can always be satisfied by a proper choice of the initial modes through the generalised eigenvalue equation, as in (14). The initial state $|\psi\rangle = |\phi_A, \phi_B\rangle$ goes through a balanced beam splitter U_{BS} , gains a relative phase φ when traveling through the two arms of the interferometer, and finally enters another beam splitter; the final state then reads

$$|\psi_\varphi\rangle = U_{BS}^\dagger e^{-i\varphi H} U_{BS} |\phi_A, \phi_B\rangle \quad (32)$$

with $H = \frac{1}{2} \left(\sum_{i=1}^d a_i^\dagger a_i - b_i^\dagger b_i \right)$, and where the transformation $U_{BS}^\dagger e^{-i\varphi H} U_{BS}$ can be described by:

$$\begin{pmatrix} \tilde{a}_j \\ \tilde{b}_j \end{pmatrix} = \frac{1}{2} \begin{pmatrix} 1 & i \\ i & 1 \end{pmatrix} \begin{pmatrix} e^{i\varphi/2} & 0 \\ 0 & e^{-i\varphi/2} \end{pmatrix} \begin{pmatrix} 1 & -i \\ -i & 1 \end{pmatrix} \begin{pmatrix} a_j \\ b_j \end{pmatrix} \quad (33)$$

where \tilde{a}_j, \tilde{b}_j are the output modes. Using this transformation we easily obtain,

$$\tilde{H} \equiv U_{BS}^\dagger H U_{BS} = \frac{i}{2} \sum_{i=1}^d \left(b_i^\dagger a_i - a_i^\dagger b_i \right). \quad (34)$$

On the other hand, $|\psi_\varphi\rangle$ can be explicitly written as:

$$\begin{aligned} |\psi_\varphi\rangle &= \sum_{\{\alpha_i\} \in \mathcal{C}(n), \{\beta_i\} \in \mathcal{C}(m)} \frac{C_{\{\beta\}}^{(B)} C_{\{\alpha\}}^{(A)}}{\sqrt{\prod_i \alpha_i! \beta_i!}} \\ &\quad \left(a_1^\dagger(\varphi) \right)^{\alpha_1} \dots \left(a_D^\dagger(\varphi) \right)^{\alpha_D} \left(b_1^\dagger(\varphi) \right)^{\beta_1} \dots \left(b_D^\dagger(\varphi) \right)^{\beta_D} |0\rangle \end{aligned} \quad (35)$$

with

$$\begin{aligned} a_j^\dagger(\varphi) &= \cos(\varphi/2) a_j^\dagger + \sin(\varphi/2) b_j^\dagger \\ b_j^\dagger(\varphi) &= -\sin(\varphi/2) a_j^\dagger + \cos(\varphi/2) b_j^\dagger. \end{aligned} \quad (36)$$

Finally, it will be useful to note that

$$\dot{a}_j^\dagger(\varphi) = \frac{1}{2} b_j^\dagger(\varphi), \quad \dot{b}_j^\dagger(\varphi) = \frac{1}{2} a_j^\dagger(\varphi). \quad (37)$$

A. Quantum Fisher Information for pure multimode states

When $|\psi\rangle = e^{-i\varphi H}$ in (28), then we have the convenient expression for the QFI: $\mathcal{Q} = 4 \left(\langle \psi_\varphi | H^2 | \psi_\varphi \rangle - (\langle \psi_\varphi | H | \psi_\varphi \rangle)^2 \right)$. Using (31) and (34), we obtain

$$\begin{aligned} \mathcal{Q} &= \langle \phi_A, \phi_B | \tilde{H}^2 | \phi_A, \phi_B \rangle - \left(\langle \phi_A, \phi_B | \tilde{H} | \phi_A, \phi_B \rangle \right)^2 \\ &= \sum_{j=1}^d [n_j(1 + m_j) + m_j(1 + n_j)] \end{aligned} \quad (38)$$

where we defined the average photon numbers $n_j \equiv \langle \phi_A | a_j^\dagger a_j | \phi_A \rangle$ and $m_j \equiv \langle \phi_B | b_j^\dagger b_j | \phi_B \rangle$. In the particular case $n_i = m_i$, e.g. for twin states, we finally obtain

$$\mathcal{Q} = 2 \sum_{j=1}^d n_j(n_j + 1). \quad (39)$$

From this expression one can immediately recover the QFI of twin Fock states $\mathcal{Q} = N(1 + N/2)$ [39], which corresponds to $d = 1$ and $n_1 = N/2$. For twin superradiant states, from our considerations of Sec. IV B we have that $2n_1 \approx 0.90N$, $2n_2 \approx 0.08N$ and $2n_3 \approx 0.02N$, from which we obtain $\mathcal{Q} \approx 0.41N^2 + N$, hence recovering our previous results [20].

More generally, (38) provides a simple and clear expression for the potential of a particular multimode state for optical interferometry, and from it we learn that

1. To obtain the QFI of a twin multimode state with $N/2$ photons in each arm, it is enough to compute the average photon number of the internal modes of each arm.
2. When the multimode state is generated through a non-linear decay as described in Section II, then our techniques enable us to compute the QFI for large photon number (N up to $N \approx 1000$).
3. Heisenberg scaling (i.e. $\mathcal{Q} \propto N^2$) is possible when the number of relevant modes is independent of N , and quantum-enhanced scaling (i.e. $\mathcal{Q} \propto N^{1+\alpha}$ with $\alpha > 0$) when the number of relevant modes grows sub-linearly with N .

B. Number resolved measurements and QFI

Although the QFI provides the maximal sensitivity of $|\psi_\varphi\rangle$ to φ , it is equally important to understand how to achieve it in practice. For that, in this section we consider number-resolved measurements in both outputs of the interferometer. In particular, we consider two types of measurements

- Mode-Number-Resolved (MNR) measurements. That is, photon measurements that are able to distinguish both the specific mode and the number of photons. In this case, defining $P_{\alpha\beta}^{(\text{MNR})}(\varphi) \equiv P(\{\alpha_j\}_{j=1}^d, \{\beta_j\}_{j=1}^d | \varphi)$ and with (30) we have

$$P_{\alpha\beta}^{(\text{MNR})}(\varphi) = |\langle \psi_\varphi | (|\{\alpha_j\}\rangle_a \otimes |\{\beta_j\}\rangle_b) |^2. \quad (40)$$

- Number-Resolved (NR) measurements. We also consider standard photon counting measurements that are not able to distinguish between the different modes. In this case the corresponding probability distribution to obtain n and m photons in each output of the interferometer reads

$$P_{nm}^{(\text{NR})}(\varphi) = \sum_{\{\alpha\} \in \mathcal{C}(n), \{\beta\} \in \mathcal{C}(m)} P_{\alpha,\beta}^{(\text{MNR})}(\varphi). \quad (41)$$

In both cases, we assume that the detector frequency-bandwidth is larger than the photonic wavepackets linewidth, which in the superradiant case scale as $\gamma \propto N/\ln N$ (see Sec. IV A and Fig. 3).

Let us now compute the CFI (26) for MNR and NR measurements when $\varphi \rightarrow 0$ by extending the considerations of [44] to multimode states. We first expand $P_{\alpha\beta}(\varphi)$ around $\varphi = 0$:

$$P_{\alpha,\beta}^{(\text{MNR})}(\varphi) = P_{\alpha,\beta}^{(\text{MNR})}(0) + \dot{P}_{\alpha,\beta}^{(\text{MNR})}(0)\varphi + \frac{1}{2}\ddot{P}_{\alpha,\beta}^{(\text{MNR})}(0)\varphi^2 \quad (42)$$

up to order $\mathcal{O}(\varphi^3)$. Let us now consider this expansion for different cases:

1. n photons in one output and m photons in the other one, i.e., $P_{\alpha\beta}^{(\text{MNR})}(\varphi)$'s such that $\{\alpha_j\} \in \mathcal{C}(n)$ and $\{\beta_j\} \in \mathcal{C}(m)$. Then using (37) we obtain, $P_{\alpha\beta}^{(\text{MNR})}(\varphi) = 1 + \mathcal{O}(\varphi^2)$, which does not contribute to (26).
2. $n \pm 1$ photons in one output and $m \mp 1$ photons in the other one. That is, $P_{\alpha\beta}^{(\text{MNR})}(\varphi)$'s such that $\{\alpha_j\} \in \mathcal{C}(n \pm 1)$ and $\{\beta_j\} \in \mathcal{C}(m \mp 1)$. Then again using (37) we have $P_{\alpha\beta}(\varphi)^{(\text{MNR})} = \frac{1}{2}\ddot{P}_{\alpha\beta}(0)\varphi^2$ with $\ddot{P}_{\alpha\beta}(0) = 2|\langle \dot{\psi}_{\varphi=0} | \{\alpha_j\}_{j=1}^d, \{\beta_j\}_{j=1}^d \rangle|^2$. This case does contribute to (26).
3. $n \pm m$ photons in one output and $m \mp m$ photons in the other one, with $m \geq 2$. Then we have, $P_{\alpha\beta}(\varphi) = \mathcal{O}(\varphi^{m+1})$, which again does not contribute to (26).

Putting together these considerations we obtain:

$$\begin{aligned} \lim_{\varphi \rightarrow 0} \mathcal{C} &= 2 \sum_{\{\alpha_j\} \in \mathcal{C}(n \pm 1), \{\beta_j\} \in \mathcal{C}(m \mp 1)} \ddot{P}_{\alpha\beta}(0) \\ &= 4 \sum_{\{\alpha_j\} \in \mathcal{C}(n \pm 1), \{\beta_j\} \in \mathcal{C}(m \mp 1)} |\langle \dot{\psi}_{\varphi=0} | \{\alpha_j\}_{j=1}^d, \{\beta_j\}_{j=1}^d \rangle|^2 \\ &= 4 \langle \dot{\psi}_{\varphi=0} | \left(\sum_{\{\alpha_j\}, \{\beta_j\}} |\{\alpha_j\}, \{\beta_j\}\rangle \langle \{\alpha_j\}, \{\beta_j\}| \right) | \dot{\psi}_{\varphi=0} \rangle \\ &= 4 \langle \dot{\psi}_{\varphi=0} | \dot{\psi}_{\varphi=0} \rangle \\ &= \lim_{\varphi \rightarrow 0} \mathcal{Q}. \end{aligned} \quad (43)$$

where in the third line we used that $|\dot{\psi}_{\varphi=0}\rangle$ has only support in the subspace of $n \pm 1$ photons in one arm and $m \mp 1$ in the

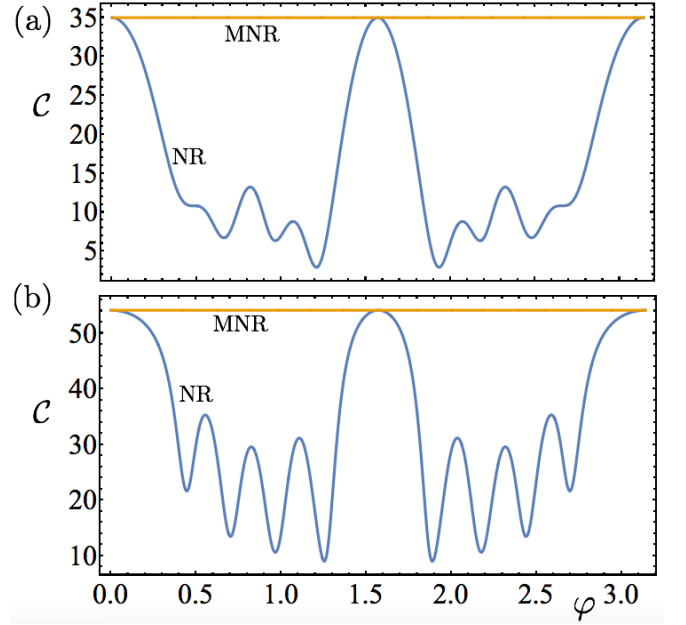


FIG. 9. Classical Fisher information for MNR measurements (in orange) and for NR measurements (in blue) when two copies of $|\psi_1\rangle$ in (44) (case (a)) or two copies of $|\psi_2\rangle$ in (45) (case (b)) enter through a MZ interferometer. The CFI for MNR measurements coincides with the QFI for all φ .

other one, and in the fourth line we used $\langle \dot{\psi}_{\varphi=0} | \dot{\psi}_{\varphi=0} \rangle = 0$. Hence, we conclude that $\mathcal{C} = \mathcal{Q}$ around $\varphi = 0$ for MNR measurements.

Crucially, the derivation (43) follows analogously for NR measurements, i.e., for the coarse-grained distribution (41). This has the very important consequence for practical implementations that experimentally one does not need to distinguish between the different modes to saturate the QFI. These conclusions hold around $\varphi = 0$, but there is in principle no reason why they should also hold for other φ . To address this point, we consider two illustrative states:

$$|\phi_1\rangle = \sum_{j=0}^n \frac{1}{\sqrt{n}} |j, n-j\rangle \quad (44)$$

$$|\phi_2\rangle = \frac{1}{\sqrt{2}} (|0, n\rangle + |n, 0\rangle), \quad (45)$$

and compute the CFI for the corresponding twin states (i.e. $|\psi_1, \psi_1\rangle$ or $|\psi_2, \psi_2\rangle$ are the input states of the MZ interferometer). In Figure 9 we plot the CFI for (44) and (45) with $n = 5$ and given MNR and NR photon measurements. We observe that $\mathcal{C} = \mathcal{Q}$ for MNR measurements whereas for the NR measurement the equality is only saturated around $\varphi = 0$ (or multiples of $\pi/2$). It is worth stressing that one can always add phase shifters to compensate for $\varphi \neq 0$ during the estimation process in order to guarantee that $\mathcal{C} = \mathcal{Q}$ for NR measurements. These are crucial considerations to take into account in implementations of quantum metrology with multimode states. It is also worth noticing that the multimode structure of the state leads to a non-trivial change of the CFI

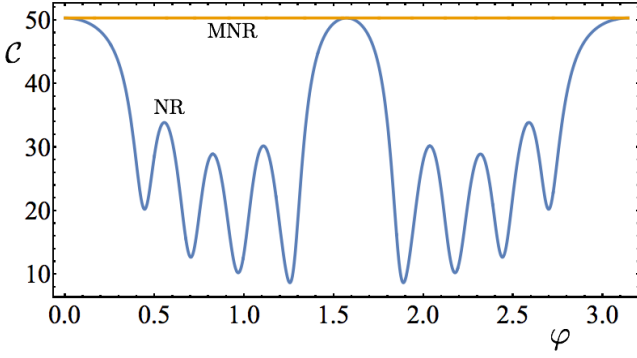


FIG. 10. Classical Fisher information for MNR measurements (in orange) and for NR measurements (in blue) for a twin superradiant state with $N = 10$ (i.e. $n = 5$).

for NR measurements, as illustrated in Figure 9.

Finally, we also compare NR and MNR measurements for twin-superradiant states as shown in Figure 10, which also illustrates the optimality of choosing $\varphi \approx 0$. To obtain the results of Figure 10, we have used the effective descriptions obtained in Section IV D which enable us to describe superradiant states through effective descriptions using a low number of modes (here we use two-mode descriptions, $d = 2$, for simplicity).

While our techniques enable us to compute the metrological properties up to hundreds of photons, we note that current experimental implementations of photon-number detectors are limited to few photons resolution ($N \leq 10$), see e.g. [45, 46]. It is also worth mentioning that recent theoretical proposals show that atoms coupled to the waveguide could also be used for photon detection up to considerably larger photon numbers [47–49], which hints to the exciting possibility that atoms suitably coupled to waveguides can be both used to generate and detect photons. In the next section we discuss a proposal for quantum metrology with superradiant states in the presence of photon loss for realistic photon numbers, namely $N \leq 10$.

C. Photon loss in the interferometer and the measurement device

Besides finding specific measurement schemes to saturate \mathcal{Q} , in practice it is also crucial to consider imperfections in the interferometer and in the measurement devices. In fact, quantum-enhancements in metrology are largely affected by imperfections (either in the interferometer or due to imperfect measurements), as photon loss prevents Heisenberg scaling for sufficiently large N [50–53]. To intuitively understand why Heisenberg scaling is lost, note that for obtaining $\mathcal{C} = \mathcal{Q}$ in (43) requires photon-measurement detectors that are capable of distinguishing a single photon (i.e. between N photons and $N \pm 1$ photons in the outcomes of the MZ interferometer); yet, in the presence of any finite photon loss (see Fig. 8), this is no longer possible when $\eta N \simeq 1$, where η is the probability of losing a photon. Still, quantum enhancements

in the presence of photon loss can appear as a better prefactor in $\mathcal{Q} \propto N$ [51–53] as classical schemes are limited by the shot-noise limit $\mathcal{Q} \leq N$. This advantage however highly depends on the state into consideration: for example, GHZ states, which are optimal in ideal conditions, are known to quickly lose any sensitivity to φ in the presence photon loss. Twin Fock States (TFS), on the other hand, are known to be a good candidate for quantum metrology even in the presence of photon loss η (quantifying the probability of losing a photon in each arm of the interferometer), as in this case the QFI becomes

$$\mathcal{Q}^{\text{TFS}} = \frac{N}{2} \frac{1 - \eta}{\eta}, \quad \text{for } \eta N \gg 1, \quad (46)$$

which is half of the optimal one in the limit of large N [51, 54]. It is also important to stress that although these considerations (e.g. (46)) are derived in the asymptotic limit ($\eta N \gg 1$), they provide valuable insights already for moderate N [51, 54]. To extend (46) and the general considerations of [50–53] to multimode states is certainly an interesting but also challenging endeavour, as the multimode structure of the state makes it difficult to diagonalise it to be able to compute \mathcal{Q} . In this Section, we instead pursue a more humble goal: We compare (twin) superradiant and Fock states for some specific case-studies of MZ interferometry and find that they perform similarly even in the presence of photon loss (which is expected as superradiant states contain $0.9N$ photons in a single mode).

We consider photon loss by adding a beam splitter with transmittivity η before each measurement apparatus (this is equivalent to placing the beam splitters before the second beam splitter of the MZ interferometer as the losses are symmetric). This is implemented by adding orthogonal modes $\{e_j\}_{j=1}^D, \{f_j\}_{j=1}^D$ and implementing the transformations \tilde{U}_{BS} :

$$\begin{pmatrix} a_j \\ e_j \end{pmatrix} \xrightarrow{\tilde{U}_{BS}} \frac{1}{\sqrt{2}} \begin{pmatrix} \sqrt{\eta} & \sqrt{1-\eta} \\ -\sqrt{1-\eta} & \sqrt{\eta} \end{pmatrix} \begin{pmatrix} a_j \\ e_j \end{pmatrix} \quad (47)$$

and

$$\begin{pmatrix} b_j \\ f_j \end{pmatrix} \xrightarrow{\tilde{U}_{BS}} \frac{1}{\sqrt{2}} \begin{pmatrix} \sqrt{\eta} & \sqrt{1-\eta} \\ -\sqrt{1-\eta} & \sqrt{\eta} \end{pmatrix} \begin{pmatrix} b_j \\ f_j \end{pmatrix}. \quad (48)$$

We again characterise the input superradiant states through the effective descriptions obtained in Section IV D with $d = 2$. These effective descriptions enable us to easily account for photon loss, which would be highly challenging through the continuous descriptions (6). Still, our results are limited to low N , both because we can only obtain the coefficients of the state for $N < 10$ (see IV D), and also because the possible outcomes of the experiment (i.e. the size of the probability distribution $P_{\alpha,\beta}^{(\text{MNR})}(\varphi)$) grows as $\mathcal{O}(N^4)$ when dealing with two-mode states in each arm of the interferometer, hence making it difficult to compute the analytical expression (26) for high N .

In Fig. 11 we show \mathcal{C} in the presence of photon loss in the measurement devices for different configurations: twin

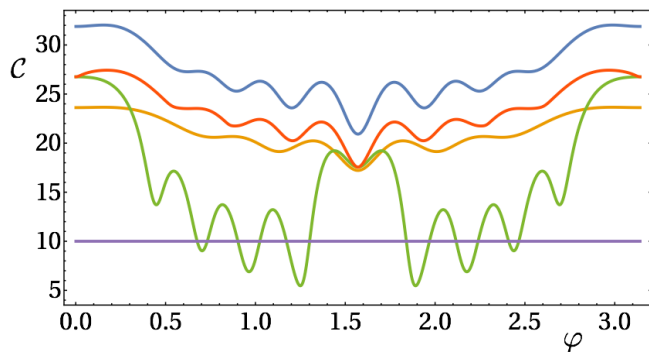


FIG. 11. Classical Fisher information in the presence of photon loss ($\eta = 0.9$) for: NR measurements in twin Fock states of $N = 8$ (orange) and $N = 10$ (blue) photons, and twin superradiant states with $N = 10$ and NR (green) and NMR (red) measurements. Finally, the straight purple line shows the classical Shot Noise Limit (SNL) corresponding to $C = N$.

Fock states of $N = 8$ (orange) and $N = 10$ (blue) photons and NR measurements, and twin superradiant states with $N = 10$ and NR (green) and NMR (red) measurements. We observe how twin superradiant states perform close to Fock states, and how NR measurements for superradiant (and hence multimode) states become optimal around $\varphi = 0$, as expected from our previous considerations. It is worth pointing out that as η increases, the optimal value moves away from $\varphi = 0$, which happens for NR and NMR measurements, and for single-mode and multimode states. These observations are confirmed by further numerical results for other values of N and η , which are shown in Appendix II. From these results, we conclude that twin-superradiant states behave fairly similar to twin-Fock states in terms of their metrological performance also in the presence of photon loss; this conclusion is indeed expected given that superradiant states contain $\approx 0.9N$ photons in a single mode.

VI. CONCLUSIONS

To sum up, we have developed the theoretical tools to characterize (i.e., compute observables) of a wide class of multimode photonic states coming from the emission of a general non-linear level structure. Besides, we provide a construc-

tive way of capturing the properties of these multimodal states with few-mode descriptions. To illustrate the potential of these tools, we have applied them to the case of superradiant photonic states, showing, for example, their observables can be captured efficiently already with two or three modes up to a large number of photons. Finally, we applied these ideas to a phase estimation proposal based on twin superradiant states and number resolved measurements. Our results suggest that twin superradiant states of N photons are a promising candidate for quantum metrology, as they perform approximately as a twin Fock state with $\approx 0.9N$ photons, which are in fact the number of photons contained in a single mode. The crucial difference is that twin superradiant states can be generated in a *deterministic* and *scalable* manner (assuming no photon loss and perfect control on the system's Hamiltonian to ensure the collective decay), in contrast to standard probabilistic methods to create Fock states, whose success probability decays exponentially with N even in ideal conditions. We hope these ideas motivate its experimental implementation in nanophotonic waveguides coupled to atoms [21–23, 28–30], artificial emitters [24, 26, 27], or molecules [25].

Our results in quantum optical interferometry are in fact general and can be applied to arbitrary multimode states with a fixed photon number. Indeed, we have considered phase estimation in a Mach-Zender interferometer and derived a simple expression for the quantum Fisher information obtained when the input state of each arm of the interferometer is a generic n -photon d -mode state, and shown that it can be saturated by number-resolved measurements that *cannot* distinguish between the different modes. This is a crucial observation for experiments, as it shows that single-mode proposals for quantum metrology, e.g. [39, 40, 44, 51, 54–56], can be naturally extended to the multimode regime without requiring extra resources in terms of the measurement devices.

VII. ACKNOWLEDGEMENTS

We thank Jan Kołodzyński for insightful discussions. We acknowledge funding from ERC Advanced Grant QENO-COBA under the EU Horizon 2020 program (Grant Agreement No. 742102). AGT acknowledges funding from project PGC2018-094792-B-I00 (MCIU/AEI/FEDER, UE), CSIC Research Platform PTI-001, and CAM/FEDER Project No. S2018/TCS-4342 (QUITEMAD-CM).

[1] Vittorio Giovannetti, Seth Lloyd, and Lorenzo Maccone, “Advances in quantum metrology,” *Nature Photonics* **5**, 222–229 (2011).
[2] Géza Tóth and Iagoba Apellaniz, “Quantum metrology from a quantum information science perspective,” *Journal of Physics A: Mathematical and Theoretical* **47**, 424006 (2014).
[3] Jonathan P. Dowling and Kaushik P. Seshadreesan, “Quantum optical technologies for metrology, sensing, and imaging,” *Journal of Lightwave Technology* **33**, 2359–2370 (2015).

[4] Rafal Demkowicz-Dobrzański, Marcin Jarzyna, and Jan Kołodzyński, “Quantum limits in optical interferometry,” in *Progress in Optics* (Elsevier, 2015) pp. 345–435.
[5] M. Dakna, J. Clausen, L. Knöll, and D.-G. Welsch, “Generation of arbitrary quantum states of traveling fields,” *Phys. Rev. A* **59**, 1658–1661 (1999).
[6] Alexei Ourjoumtsev, Rosa Tualle-Broui, Julien Laurat, and Philippe Grangier, “Generating optical schrödinger kittens for quantum information processing,” *Science* **312**, 83–86 (2006).

- [7] Edo Waks, Eleni Diamanti, and Yoshihisa Yamamoto, “Generation of photon number states,” *New Journal of Physics* **8**, 4 (2006).
- [8] Alessandro Zavatta, Valentina Parigi, and Marco Bellini, “Toward quantum frequency combs: Boosting the generation of highly nonclassical light states by cavity-enhanced parametric down-conversion at high repetition rates,” *Phys. Rev. A* **78**, 033809 (2008).
- [9] Xi-Lin Wang, Luo-Kan Chen, W. Li, H.-L. Huang, C. Liu, C. Chen, Y.-H. Luo, Z.-E. Su, D. Wu, Z.-D. Li, H. Lu, Y. Hu, X. Jiang, C.-Z. Peng, L. Li, N.-L. Liu, Yu-Ao Chen, Chao-Yang Lu, and Jian-Wei Pan, “Experimental ten-photon entanglement,” *Phys. Rev. Lett.* **117**, 210502 (2016).
- [10] D Porras and JI Cirac, “Collective generation of quantum states of light by entangled atoms,” *Physical Review A* **78**, 053816 (2008).
- [11] Karel Lemr and Jaromír Fiurášek, “Conditional preparation of arbitrary superpositions of atomic dicke states,” *Phys. Rev. A* **79**, 043808 (2009).
- [12] L.-M. Duan and H. J. Kimble, “Efficient engineering of multiatom entanglement through single-photon detections,” *Phys. Rev. Lett.* **90**, 253601 (2003).
- [13] A. González-Tudela, V. Paulisch, D. E. Chang, H. J. Kimble, and J. I. Cirac, “Deterministic generation of arbitrary photonic states assisted by dissipation,” *Phys. Rev. Lett.* **115**, 163603 (2015).
- [14] A. González-Tudela, V. Paulisch, H. J. Kimble, and J. I. Cirac, “Efficient multiphoton generation in waveguide quantum electrodynamics,” *Phys. Rev. Lett.* **118**, 213601 (2017).
- [15] Subhadeep Gupta, Kevin L. Moore, Kater W. Murch, and Dan M. Stamper-Kurn, “Cavity nonlinear optics at low photon numbers from collective atomic motion,” *Phys. Rev. Lett.* **99**, 213601 (2007).
- [16] A. Dousse, J. Suffczyński, A. Beveratos, O. Krebs, A. Lemaître, I. Sagnes, J. Bloch, P. Voisin, and P. Senellart, “Ultrabright source of entangled photon pairs,” *Nature* **466**, 217 (2010).
- [17] Yasutomo Ota, Satoshi Iwamoto, Naoto Kumagai, and Yasuhiko Arakawa, “Spontaneous two-photon emission from a single quantum dot,” *Phys. Rev. Lett.* **107**, 233602 (2011).
- [18] M. D. Lukin and A. Imamoglu, “Controlling photons using electromagnetically induced transparency,” *Nature* **413**, 273 (2001).
- [19] M. Saffman, T. G. Walker, and K. Mølmer, “Quantum information with rydberg atoms,” *Rev. Mod. Phys.* **82**, 2313–2363 (2010).
- [20] V. Paulisch, M. Perarnau-Llobet, A. González-Tudela, and J. I. Cirac, “Quantum metrology with one-dimensional superradiant photonic states,” *Phys. Rev. A* **99**, 043807 (2019).
- [21] E. Vetsch, D. Reitz, G. Sagué, R. Schmidt, S. T. Dawkins, and A. Rauschenbeutel, “Optical interface created by laser-cooled atoms trapped in the evanescent field surrounding an optical nanofiber,” *Phys. Rev. Lett.* **104**, 203603 (2010).
- [22] J. D. Thompson, T. G. Tiecke, N. P. de Leon, J. Feist, A. V. Akimov, M. Gullans, A. S. Zibrov, V. Vuletic, and M. D. Lukin, “Coupling a single trapped atom to a nanoscale optical cavity,” *Science* **340**, 1202–1205 (2013).
- [23] A. Goban, C.-L. Hung, S.-P. Yu, J.D. Hood, J.A. Muniz, J.H. Lee, M.J. Martin, A.C. McClung, K.S. Choi, D.E. Chang, O. Painter, and H.J. Kimble, “Atom-light interactions in photonic crystals,” *Nat. Commun.* **5**, 3808 (2014).
- [24] A. Laucht, S. Pütz, T. Günthner, N. Hauke, R. Saive, S. Frédérick, M. Bichler, M.-C. Amann, A. W. Holleitner, M. Kaniber, and J. J. Finley, “A Waveguide-Coupled On-Chip Single-Photon Source,” *Phys. Rev. X* **2**, 011014 (2012).
- [25] Sanli Faez, Pierre Türschmann, Harald R. Haakh, Stephan Götzinger, and Vahid Sandoghdar, “Coherent interaction of light and single molecules in a dielectric nanoguide,” *Phys. Rev. Lett.* **113**, 213601 (2014).
- [26] Peter Lodahl, Sahand Mahmoodian, and Søren Stobbe, “Interfacing single photons and single quantum dots with photonic nanostructures,” *Rev. Mod. Phys.* **87**, 347–400 (2015).
- [27] Alp Sipahigil, RE Evans, DD Sukachev, MJ Burek, J Borregaard, MK Bhaskar, CT Nguyen, JL Pacheco, HA Atikian, C Meuwly, *et al.*, “An integrated diamond nanophotonics platform for quantum optical networks,” *Science*, aah6875 (2016).
- [28] Neil V. Corzo, Baptiste Gouraud, Aveek Chandra, Akihisa Goban, Alexandra S. Sheremet, Dmitriy V. Kupriyanov, and Julien Laurat, “Large bragg reflection from one-dimensional chains of trapped atoms near a nanoscale waveguide,” *Phys. Rev. Lett.* **117**, 133603 (2016).
- [29] H. L. Sørensen, J.-B. Béguin, K. W. Kluge, I. Iakoupov, A. S. Sørensen, J. H. Müller, E. S. Polzik, and J. Appel, “Coherent backscattering of light off one-dimensional atomic strings,” *Phys. Rev. Lett.* **117**, 133604 (2016).
- [30] P Solano, P Barberis-Blostein, FK Fatemi, LA Orozco, and SL Rolston, “Super-radiance reveals infinite-range dipole interactions through a nanofiber,” *Nature communications* **8**, 1857 (2017).
- [31] H.L. Sørensen, J.-B. Béguin, K.W. Kluge, I. Iakoupov, A. S. Sørensen, J.H. Müller, E. S. Polzik, and J. Appel, “Coherent backscattering of light off one-dimensional atomic strings,” *Phys. Rev. Lett.* **117**, 133604 (2016).
- [32] R. H. Dicke, “Coherence in Spontaneous Radiation Processes,” *Phys. Rev.* **93**, 99 (1954).
- [33] Andreas Christ and Christine Silberhorn, “Limits on the deterministic creation of pure single-photon states using parametric down-conversion,” *Phys. Rev. A* **85**, 023829 (2012).
- [34] Johannes Tiedau, Tim J Bartley, Georg Harder, Adriana E Lita, Sae Woo Nam, Thomas Gerrits, and Christine Silberhorn, “On the scalability of parametric down-conversion for generating higher-order fock states,” arXiv:1901.03237 (2019).
- [35] N Quesada, LG Helt, J Izaac, JM Arrazola, R Shahrokhshahi, CR Myers, and KK Sabapathy, “Simulating realistic non-gaussian state preparation,” arXiv:1905.07011 (2019).
- [36] Ben Q. Baragiola, Robert L. Cook, Agata M. Brańczyk, and Joshua Combes, “*n*-photon wave packets interacting with an arbitrary quantum system,” *Phys. Rev. A* **86**, 013811 (2012).
- [37] Alexander Holm Kiilerich and Klaus Mølmer, “Input-output theory with quantum pulses,” *Phys. Rev. Lett.* **123**, 123604 (2019).
- [38] T. Shi, D.E. Chang, and J.I. Cirac, “Generalized master equation,” in preparation.
- [39] M. J. Holland and K. Burnett, “Interferometric detection of optical phase shifts at the heisenberg limit,” *Phys. Rev. Lett.* **71**, 1355–1358 (1993).
- [40] R. A. Campos, Christopher C. Gerry, and A. Benmoussa, “Optical interferometry at the heisenberg limit with twin fock states and parity measurements,” *Phys. Rev. A* **68**, 023810 (2003).
- [41] Samuel L. Braunstein and Carlton M. Caves, “Statistical distance and the geometry of quantum states,” *Phys. Rev. Lett.* **72**, 3439–3443 (1994).
- [42] C. W. Helstrom, *Quantum Detection and Estimation Theory* (Elsevier Science, 1976).
- [43] Alexander S. Holevo, *Probabilistic and Statistical Aspects of Quantum Theory (Statistics & Probability) (English and Russian Edition)* (Elsevier Science, 1982).
- [44] Luca Pezzé and Augusto Smerzi, “Ultrasensitive two-mode interferometry with single-mode number squeezing,” *Phys. Rev.*

- Lett. **110**, 163604 (2013).
- [45] Robert H. Hadfield, “Single-photon detectors for optical quantum information applications,” *Nature Photonics* **3**, 696–705 (2009).
- [46] Mattias Jönsson and Gunnar Björk, “Evaluating the performance of photon-number-resolving detectors,” *Phys. Rev. A* **99**, 043822 (2019).
- [47] B. Peropadre, G. Romero, G. Johansson, C. M. Wilson, E. Solano, and J. J. García-Ripoll, “Approaching perfect microwave photodetection in circuit qed,” *Phys. Rev. A* **84**, 063834 (2011).
- [48] G. Romero, J. J. García-Ripoll, and E. Solano, “Microwave photon detector in circuit qed,” *Phys. Rev. Lett.* **102**, 173602 (2009).
- [49] Daniel Malz and J Ignacio Cirac, “Number-resolving photon detectors with atoms coupled to waveguides,” arXiv preprint arXiv:1906.12296 (2019).
- [50] Akio Fujiwara and Hiroshi Imai, “A fibre bundle over manifolds of quantum channels and its application to quantum statistics,” *Journal of Physics A: Mathematical and Theoretical* **41**, 255304 (2008).
- [51] Sergey Knysh, Vadim N. Smelyanskiy, and Gabriel A. Durkin, “Scaling laws for precision in quantum interferometry and the bifurcation landscape of the optimal state,” *Phys. Rev. A* **83**, 021804 (2011).
- [52] BM Escher, RL de Matos Filho, and L Davidovich, “General framework for estimating the ultimate precision limit in noisy quantum-enhanced metrology,” *Nature Physics* **7**, 406 (2011).
- [53] Rafał Demkowicz-Dobrzański, Jan Kołodyński, and Mădălin Guță, “The elusive heisenberg limit in quantum-enhanced metrology,” *Nature communications* **3**, 1063 (2012).
- [54] Sergey I Knysh, Edward H Chen, and Gabriel A Durkin, “True limits to precision via unique quantum probe,” arXiv preprint arXiv:1402.0495 (2014).
- [55] Holger F. Hofmann, “All path-symmetric pure states achieve their maximal phase sensitivity in conventional two-path interferometry,” *Phys. Rev. A* **79**, 033822 (2009).
- [56] M. Ozmaniec, R. Augusiak, C. Gogolin, J. Kołodyński, A. Acín, and M. Lewenstein, “Random bosonic states for robust quantum metrology,” *Phys. Rev. X* **6**, 041044 (2016).

APPENDIX

I. RECURRENCE RELATIONS

Here we build recurrence relations to compute

$$f(\{x_j, y_j, \tilde{x}_j, \tilde{y}_j\}_{j=1}^n) = \langle \phi^{(N)} | b_{x_1, y_1} \dots b_{x_n, y_n} b_{\tilde{x}_1, \tilde{y}_1}^\dagger \dots b_{\tilde{x}_n, \tilde{y}_n}^\dagger | \phi^{(N)} \rangle. \quad (1)$$

As the derivation is rather non-trivial, for clarity we will start by computing simple but relevant cases where $n = 0, 1, 2$ before deriving a general relation for (1).

Along the derivation we will use that from (8) it follows that

$$\langle 0 | b_{x_1, y_1} b_{\tilde{x}_1, \tilde{y}_1}^\dagger | 0 \rangle = \frac{2\sqrt{x_1 \tilde{x}_1}}{x_1 + \tilde{x}_1 + 2i(\tilde{y}_1 - y_1)} \quad (2)$$

and similarly

$$[b_{x_1, y_1}, b_{\tilde{x}_1, \tilde{y}_1}^\dagger] = \frac{2\sqrt{x_1 \tilde{x}_1}}{x_1 + \tilde{x}_1 + 2i(\tilde{y}_1 - y_1)}. \quad (3)$$

A. Normalisation

It is instructive to first check that $|\phi^{(N)}\rangle$ is normalised. We want to compute,

$$\langle \phi^{(N)} | \phi^{(N)} \rangle = \frac{1}{(N!)^2} \int \dots \int_0^\infty A_{t_1 \dots t_N} A_{s_1 \dots s_N}^* \left(\prod_{j,k=1}^N dt_j ds_j \right) \langle 0 | a_{s_1} \dots a_{s_N} a_{t_1}^\dagger \dots a_{t_N}^\dagger | 0 \rangle \quad (4)$$

Using the symmetry of $A_{t_1 \dots t_N}$ under permutations over $\{t_j\}$ and the commutation relation (8), we arrive at

$$\langle \phi^{(N)} | \phi^{(N)} \rangle = \frac{1}{N!} \int \dots \int_0^\infty \left(\prod_{j,k=1}^N dt_j \right) |A_{t_1 \dots t_N}|^2. \quad (5)$$

In order to solve this integral, which includes a time-ordering operation \mathcal{T} , we split the integral as a sum of integrals using

$$\int_0^\infty \int_0^\infty dx dy \mathcal{T} \langle \mathcal{O}_x \mathcal{O}_y \rangle = \int_0^\infty dy \int_y^\infty dx \langle \mathcal{O}_x \mathcal{O}_y \rangle + \int_0^\infty dx \int_x^\infty dy \langle \mathcal{O}_y \mathcal{O}_x \rangle. \quad (6)$$

There are $N!$ such integrals, and they are equivalent. Hence we have that

$$\langle \phi^{(N)} | \phi^{(N)} \rangle = \int_0^\infty dt_N \dots \int_{t_3}^\infty dt_2 \int_{t_2}^\infty dt_1 \prod_{j=1}^N \gamma_j \exp[(\gamma_{j-1} - \gamma_j)t_j]. \quad (7)$$

This integral can be easily worked out using $\int_s^\infty ds e^{-at} = e^{-as}/a$, which leads to the desired result

$$\langle \phi^{(N)} | \phi^{(N)} \rangle = 1. \quad (8)$$

B. Average photon number

We first consider $f(x_1, y_1, \tilde{x}_1, \tilde{y}_1)$. Before proceeding to its calculation, first note

$$f(x_1, y_1, \tilde{x}_1, \tilde{y}_1) = \frac{2\sqrt{x_1\tilde{x}_1}}{x_1 + \tilde{x}_1 + 2i(\tilde{y}_1 - y_1)} + \langle \phi^{(N)} | b_{\tilde{x}_1, \tilde{y}_1}^\dagger b_{x_1, y_1} | \phi^{(N)} \rangle. \quad (9)$$

Using (8) and (2) and the symmetry of $A_{t_1 \dots t_N}$ over permutations, we first have

$$f(x_1, y_1, \tilde{x}_1, \tilde{y}_1) = \frac{2\sqrt{x_1\tilde{x}_1}}{x_1 + \tilde{x}_1 + 2i(\tilde{y}_1 - y_1)} + NI_1^{(N)}(x_1, y_1, x_2, y_2) \quad (10)$$

with

$$I_1^{(N)}(x_1, y_1, \tilde{x}_1, \tilde{y}_1) = \frac{1}{N!} \int_0^\infty \dots \int_0^\infty \prod_{j=2}^N dt_j \, du \, dv \, A_{ut_2 \dots t_N} A_{vt_2 \dots t_N}^* B_u^{(x_1, y_1)*} B_v^{(\tilde{x}_1, \tilde{y}_1)}. \quad (11)$$

This integral is challenging to compute because of the time-ordering \mathcal{T} . We will compute the integral through a recurrence relation. The rough idea is as follows: first one splits the integral as a sum of integrals using (6). Since the number of integrals increases exponentially with N , it is crucial to use that when any of the t_j 's is integrated, the resulting integral is the same due to the symmetry of A under permutations. This allows us to keep the computation efficient, as the number of integrals grows linearly with N . Let us implement this idea by developing a recurrence relation where each step corresponds to an integration through one of the variables of integration (u, v, t_1, t_2, \dots). Let us start by defining the integrals

$$\begin{aligned} F_{1,1}^{(N-j)} &= \int_0^\infty \dots \int_0^\infty \left(\prod_{k=j+1}^N dt_k \right) du \, dv \, e^{-c_{1,1}^{(N-j)} \max\{t_j, u, v\}} \mathcal{T} \langle \varphi_j | \mathcal{O}_u \mathcal{O}_{t_{j+1}} \dots \mathcal{O}_{t_N} | \varphi_N \rangle (\langle \varphi_j | \mathcal{O}_v \mathcal{O}_{t_{j+1}} \dots \mathcal{O}_{t_N} | \varphi_N \rangle)^* B_u^{(x_1, y_1)*} B_v^{(\tilde{x}_1, \tilde{y}_1)} \\ F_{1,0}^{(N-j)} &= \int_0^\infty \dots \int_0^\infty \left(\prod_{k=j+1}^N dt_k \right) du \, dv \, e^{-c_{1,0}^{(N-j)} \max\{t_j, u\}} \mathcal{T} \langle \varphi_j | \mathcal{O}_u \mathcal{O}_{t_{j+1}} \dots \mathcal{O}_{t_N} | \varphi_N \rangle (\langle \varphi_j | \mathcal{O}_{t_{j+1}} \dots \mathcal{O}_{t_N} | \varphi_N \rangle)^* B_u^{(x_1, y_1)*} \\ F_{0,1}^{(N-j)} &= \int_0^\infty \dots \int_0^\infty \left(\prod_{k=j+1}^N dt_k \right) du \, dv \, e^{-c_{0,1}^{(N-j)} \max\{t_j, v\}} \mathcal{T} \langle \varphi_j | \mathcal{O}_{t_{j+1}} \dots \mathcal{O}_{t_N} | \varphi_N \rangle (\langle \varphi_j | \mathcal{O}_v \mathcal{O}_{t_{j+1}} \dots \mathcal{O}_{t_N} | \varphi_N \rangle)^* B_v^{(\tilde{x}_1, \tilde{y}_1)} \\ F_{0,0}^{(N-j)} &= \int_0^\infty \dots \int_0^\infty \left(\prod_{k=j+1}^N dt_k \right) du \, dv \, e^{-c_{0,0}^{(N-j)} \max\{t_j\}} \mathcal{T} \langle \varphi_j | \mathcal{O}_{t_{j+1}} \dots \mathcal{O}_{t_N} | \varphi_N \rangle (\langle \varphi_j | \mathcal{O}_{t_{j+1}} \dots \mathcal{O}_{t_N} | \varphi_N \rangle)^* \end{aligned} \quad (12)$$

with

$$\begin{aligned} c_{1,1}^{(N-j)} &= \gamma_{j-1} \\ c_{1,0}^{(N-j)} &= \frac{1}{2}\tilde{x}_1 + \frac{1}{2}(\gamma_{j-1} + \gamma_j) - i(\tilde{y}_1 - (\omega_{j-1} - \omega_j)) \\ c_{0,1}^{(N-j)} &= \frac{1}{2}x_1 + \frac{1}{2}(\gamma_{j-1} + \gamma_j) + i(y_1 - (\omega_{j-1} - \omega_j)) \\ c_{0,0}^{(N-j)} &= \frac{1}{2}(x_1 + \tilde{x}_1) + \gamma_j + i(y_1 - \tilde{y}_1), \end{aligned} \quad (13)$$

with $j = 1, \dots, N$. Note that

$$I_1^{(N)}(x_1, y_1, \tilde{x}_1, \tilde{y}_1) = \frac{1}{N!} F_{1,1}^{(N-1)}. \quad (14)$$

We can then compute $F_{1,1}^{(N-1)}$ by noting the following recurrence relation (with $j = 1, \dots, N$):

$$\begin{aligned} F_{1,1}^{(N-j)} &= \frac{(N-j)\gamma_j}{c_{1,1}^{(N-j-1)}} F_{1,1}^{(N-j-1)} + \frac{\sqrt{\tilde{x}_1\gamma_j}}{c_{1,0}^{(N-j)}} F_{1,0}^{(N-j)} + \frac{\sqrt{x_1\gamma_j}}{c_{0,1}^{(N-j)}} F_{0,1}^{(N-j)} \\ F_{1,0}^{(N-j)} &= \frac{(N-j)\sqrt{\gamma_j\gamma_{j+1}}}{c_{0,1}^{(N-j-1)}} F_{1,0}^{(N-j-1)} + \frac{\sqrt{x_1\gamma_j}}{c_{0,0}^{(N-j)}} F_{0,0}^{(N-j)} \\ F_{0,1}^{(N-j)} &= \frac{(N-j)\sqrt{\gamma_j\gamma_{j+1}}}{c_{1,0}^{(N-j-1)}} F_{0,1}^{(N-j-1)} + \frac{\sqrt{\tilde{x}_1\gamma_j}}{c_{0,0}^{(N-j)}} F_{0,0}^{(N-j)} \\ F_{0,0}^{(N-j)} &= \frac{(N-j)\gamma_{j+1}}{c_{0,0}^{(N-j-1)}} F_{0,0}^{(N-j-1)}, \end{aligned} \quad (15)$$

together with

$$F_{0,0}^{(0)} = 1. \quad (16)$$

Next, the idea is to express (15) as a matrix multiplication. In particular, let us define a matrix of size $(4N)^2$ given by:

$$M = \begin{bmatrix} M_{11} & M_{12} & M_{13} & M_{14} \\ M_{21} & M_{22} & M_{23} & M_{24} \\ M_{31} & M_{32} & M_{33} & M_{34} \\ M_{41} & M_{42} & M_{43} & M_{44} \end{bmatrix}$$

where M_{ij} are matrices of size N^2 with entries $M_{ij}[[k, l]]$ given by

$$\begin{aligned} M_{11}[[j+1, j]] &= j \frac{\gamma_{N-j+1}}{c_{0,0}^{(j-1)}} \quad \text{with } j = 1, \dots, N-1, \quad \text{and } 0 \text{ otherwise} \\ M_{22}[[j+1, j]] &= j \frac{\sqrt{\gamma_{N-j}\gamma_{N-j+1}}}{c_{1,0}^{(j-1)}} \quad \text{with } j = 1, \dots, N-1, \quad \text{and } 0 \text{ otherwise} \\ M_{33}[[j+1, j]] &= j \frac{\sqrt{\gamma_{N-j}\gamma_{N-j+1}}}{c_{0,1}^{(j-1)}} \quad \text{with } j = 1, \dots, N-1, \quad \text{and } 0 \text{ otherwise} \\ M_{44}[[j+1, j]] &= j \frac{\gamma_{N-j}}{c_{1,1}^{(j-1)}} \quad \text{with } j = 1, \dots, N-1, \quad \text{and } 0 \text{ otherwise} \\ M_{21}[[j, j]] &= \frac{\sqrt{\gamma_{N-j}x}}{c_{0,0}^{(j)}} \quad \text{with } j = 1, \dots, N, \quad \text{and } 0 \text{ otherwise} \\ M_{31}[[j, j]] &= \frac{\sqrt{\gamma_{N-j}y}}{c_{0,0}^{(j)}} \quad \text{with } j = 1, \dots, N, \quad \text{and } 0 \text{ otherwise} \\ M_{42}[[j, j]] &= \frac{\sqrt{\gamma_{N-j}y}}{c_{1,0}^{(j)}} \quad \text{with } j = 1, \dots, N, \quad \text{and } 0 \text{ otherwise} \\ M_{43}[[j, j]] &= \frac{\sqrt{\gamma_{N-j}x}}{c_{0,1}^{(j)}} \quad \text{with } j = 1, \dots, N, \quad \text{and } 0 \text{ otherwise} \end{aligned} \quad (17)$$

and the remaining submatrices are zero. Defining the initial vector: $\vec{v}_0 = \{1, 0, \dots, 0\}$, one finds that

$$\vec{v}_f = M^{N+1} \cdot \vec{v}_0 \quad (18)$$

where

$$\vec{v}_f = \{0, \dots, 0, F_{1,1}^{(N-1)}\}, \quad (19)$$

which provides the desired result. When computing this numerically, it is convenient to compute instead

$$\vec{v}_f = \left(\prod_{j=1}^N \frac{M}{j} \right) \cdot M \cdot \vec{v}_0 \quad (20)$$

which directly provides $I_1^{(N)}(x_1, y_1, \tilde{x}_1, \tilde{y}_1)$ in (14).

C. Two-photon correlators

Let us now move to the computation of

$$f(\{x_j, y_j, \tilde{x}_j, \tilde{y}_j\}_{j=1}^2) = \langle \phi^{(N)} | b_{x_1, y_1} b_{x_2, y_2} b_{\tilde{x}_1, \tilde{y}_1}^\dagger b_{\tilde{x}_2, \tilde{y}_2}^\dagger | \phi^{(N)} \rangle. \quad (21)$$

Using (8) and (2) and the symmetry of $A_{t_1 \dots t_N}$ over permutations, we arrive at

$$\begin{aligned} f(\{x_j, y_j, \tilde{x}_j, \tilde{y}_j\}_{j=1}^2) &= \frac{2\sqrt{x_1 \tilde{x}_1 y_1 \tilde{y}_1}}{(x_1 + \tilde{x}_1 + 2i(\tilde{y}_1 - y_1))(x_2 + \tilde{x}_2 + 2i(\tilde{y}_2 - y_2))} + \frac{2\sqrt{x_1 \tilde{x}_1 y_1 \tilde{y}_1}}{(x_1 + \tilde{x}_1 + 2i(\tilde{y}_2 - y_1))(x_2 + \tilde{x}_1 + 2i(\tilde{y}_1 - y_2))} \\ &+ N \frac{2\sqrt{x_1 \tilde{x}_1}}{x_1 + \tilde{x}_1 + 2i(\tilde{y}_1 - y_1)} I_1^{(N)}(x_2, y_2, \tilde{x}_2, \tilde{y}_2) + N \frac{2\sqrt{x_1 \tilde{x}_2}}{x_1 + \tilde{x}_2 + 2i(\tilde{y}_2 - y_1)} I_1^{(N)}(x_2, y_2, \tilde{x}_1, \tilde{y}_1) \\ &+ N \frac{2\sqrt{x_2 \tilde{x}_1}}{x_2 + \tilde{x}_1 + 2i(\tilde{y}_1 - y_2)} I_1^{(N)}(x_1, y_1, \tilde{x}_2, \tilde{y}_2) + N \frac{2\sqrt{x_2 \tilde{x}_2}}{x_2 + \tilde{x}_2 + 2i(\tilde{y}_2 - y_2)} I_1^{(N)}(x_1, y_1, \tilde{x}_1, \tilde{y}_1) \\ &+ N(N-1) I_2^{(N)}(x_1, y_1, x_2, y_2, \tilde{x}_1, \tilde{y}_1, \tilde{x}_2, \tilde{y}_2) \end{aligned} \quad (22)$$

where we have defined

$$\begin{aligned} I_2^{(N)}(x_1, y_1, x_2, y_2, \tilde{x}_1, \tilde{y}_1, \tilde{x}_2, \tilde{y}_2) &= \\ \frac{1}{N!} \int_0^\infty \dots \int_0^\infty \left(\prod_{j=3}^N dt_j \right) du_1 du_2 dv_1 dv_2 A_{u_1 u_2 t_3 \dots t_N} A_{v_1 v_2 t_3 \dots t_N}^* B_{u_1}^{(x_1, y_1)*} B_{u_2}^{(x_2, y_2)*} B_{v_1}^{(\tilde{x}_1, \tilde{y}_1)} B_{v_2}^{(\tilde{x}_2, \tilde{y}_2)} \end{aligned} \quad (23)$$

in analogy with (11). Identifying

$$I_2^{(N)}(x_1, y_1, x_2, y_2, \tilde{x}_1, \tilde{y}_1, \tilde{x}_2, \tilde{y}_2) = \frac{F_{1,1,1,1}^{(N-2)}}{N!} \quad (24)$$

we find the following recurrence relation (a natural extension of (15)),

$$\begin{aligned} F_{1-s_1, 1-s_2, 1-t_1, 1-t_2}^{(N-1-k)} &= \delta_{s_1, 0} F_{0, 1-s_2, 1-t_1, 1-t_2}^{(N-1-k)} \frac{\sqrt{x_1 \gamma_{k+s_2}}}{c_{0, 1-s_2, 1-t_1, 1-t_2}^{(N-1-k)}} + \delta_{s_2, 0} F_{1-s_1, 0, 1-t_1, 1-t_2}^{(N-1-k)} \frac{\sqrt{x_2 \gamma_{k+s_1}}}{c_{0, 1-s_2, 1-t_1, 1-t_2}^{(N-1-k)}} \\ &+ \delta_{t_1, 0} F_{1-s_1, 1-s_2, 0, 1-t_2}^{(N-1-k)} \frac{\sqrt{\tilde{x}_1 \gamma_{k+t_2}}}{c_{1-s_1, 1-s_2, 0, 1-t_2}^{(N-1-k)}} + \delta_{t_2, 0} F_{1-s_1, 1-s_2, 1-t_1, 0}^{(N-1-k)} \frac{\sqrt{\tilde{x}_2 \gamma_{k+t_1}}}{c_{1-s_1, 1-s_2, 1-t_1, 0}^{(N-1-k)}} \\ &+ (N-k-1) F_{1-s_1, 1-s_2, 1-t_1, 1-t_2}^{(N-2-k)} \frac{\sqrt{\gamma_{k+s_1+s_2} \gamma_{k+t_1+t_2}}}{c_{1-s_1, 1-s_2, 1-t_1, 1-t_2}^{(N-2-k)}} \end{aligned} \quad (25)$$

with $k = 1, \dots, N-2$, and

$$F_{0,0,0,0}^{(0)} = 1, \quad (26)$$

and

$$c_{1-s_1, 1-s_2, 1-t_1, 1-t_2}^{(N-2-k)} = \sum_{i=1}^2 s_i \left(\frac{x_i}{2} + i y_i \right) + t_i \left(\frac{\tilde{x}_i}{2} - i \tilde{y}_i \right) + \frac{1}{2} (\gamma_{s_1+s_2+k} + \gamma_{t_1+t_2+k}) + i(\omega_{k+t_1+t_2} - \omega_{k+s_1+s_2}). \quad (27)$$

In order to compute the recurrence relation (25) as a matrix multiplication, it is convenient to define basis vectors: $|k, s_1, s_2, t_1, t_2\rangle$ with $k = \{1, \dots, N-1\}$, and $s_1, s_2, t_1, t_2 \in \{0, 1\}$. Then, the idea is to define a matrix M that satisfies,

$$\begin{aligned} M|k, s_1, s_2, t_1, t_2\rangle &= C_{k-1, s_1, s_2, t_1, t_2}|k-1, s_1, s_2, t_1, t_2\rangle + C_{k, s_1-1, s_2, t_1, t_2}|k, s_1-1, s_2, t_1, t_2\rangle \\ &+ C_{k, s_1, s_2-1, t_1, t_2}|k, s_1, s_2-1, t_1, t_2\rangle + C_{k, s_1, s_2, t_1-1, t_2}|k, s_1, s_2, t_1-1, t_2\rangle \\ &+ C_{k, s_1, s_2, t_1, t_2-1}|k, s_1, s_2, t_1, t_2-1\rangle \end{aligned} \quad (28)$$

with

$$\begin{aligned} C_{k-1, s_1, s_2, t_1, t_2} &= (N-k-1) \frac{\sqrt{\gamma_{k+s_1+s_2} \gamma_{k+t_1+t_2}}}{C_{1-s_1, 1-s_2, 1-t_1, 1-t_2}^{(N-2-k)}} \\ C_{k, s_1-1, s_2, t_1, t_2} &= \delta_{s_1, 0} \frac{\sqrt{x_1 \gamma_{k+s_2}}}{C_{0, 1-s_2, 1-t_1, 1-t_2}^{(N-1-k)}} \\ C_{k, s_1, s_2-1, t_1, t_2} &= \delta_{s_2, 0} \frac{\sqrt{x_2 \gamma_{k+s_1}}}{C_{0, 1-s_2, 1-t_1, 1-t_2}^{(N-1-k)}} \\ C_{k, s_1, s_2, t_1-1, t_2} &= \delta_{t_1, 0} \frac{\sqrt{y_1 \gamma_{k+t_2}}}{C_{1-s_1, 1-s_2, 0, 1-t_2}^{(N-1-k)}} \\ C_{k, s_1, s_2, t_1, t_2-1} &= \delta_{t_2, 0} \frac{\sqrt{y_2 \gamma_{k+t_1}}}{C_{1-s_1, 1-s_2, 1-t_1, 0}^{(N-1-k)}} \end{aligned} \quad (29)$$

which provide the coefficients of M . Then, notice that from (25) one obtains,

$$M^{N+2}|N-1, 1, 1, 1, 1\rangle = F_{1,1,1,1}^{(N-2)}|1, 0, 0, 0, 0\rangle, \quad (30)$$

which gives the desired result. Note that the matrices M are now of size $(2^4(N-1))^2$.

D. Higher order terms

Given these previous considerations, it is in principle not difficult (but quite tedious) to extend these techniques to higher-order correlators of the form $\langle \phi^{(N)} | b_{x_1, y_1} \dots b_{x_n, y_n} b_{\tilde{x}_1, \tilde{y}_1}^\dagger \dots b_{\tilde{x}_n, \tilde{y}_n}^\dagger | \phi^{(N)} \rangle$. Essentially, following the previous considerations we need to compute integrals of the form

$$I_n^{(N)}(\{x_j, y_j, \tilde{x}_j, \tilde{y}_j\}_{j=1}^n) = \frac{1}{N!} \int_0^\infty \dots \int_0^\infty \left(\prod_{j=n+1}^N dt_j \right) \left(\prod_{j=1}^n du_j dv_j B_{u_j}^{(x_j, y_j)*} B_{v_j}^{(\tilde{x}_j, \tilde{y}_j)} \right) A_{u_1 \dots u_n t_{n+1} \dots t_N} A_{v_1 \dots v_n t_{n+1} \dots t_N}^* \quad (31)$$

In complete analogy with the previous considerations, we can define

$$I_n^{(N)}(\{x_j, y_j, \tilde{x}_j, \tilde{y}_j\}_{j=1}^n) = \frac{F_{1, \dots, 1}^{(N-n)}}{N!} \quad (32)$$

and the following recurrence relation can be derived (a natural extension of (25)),

$$\begin{aligned} F_{\{1-s_i\}_{i=1}^n, \{1-t_i\}_{i_1}^n}^{(N-n+1-k)} &= \sum_{j=1}^n \delta_{s_j, 0} F_{\{1-s_i\}_{i=1}^{j-1}, 0, \{1-s_i\}_{i=j+1}^n, \{1-t_i\}_{i_1}^n}^{(N-n+1-k)} \frac{\sqrt{x_j \gamma_{k+\sum_{j=1}^n s_j}}}{C_{\{1-s_i\}_{i=1}^j, 0, \{1-s_i\}_{i=j+1}^n, \{1-t_i\}_{i_1}^n}^{(N-n+1-k)}} \\ &+ \sum_{j=1}^n \delta_{t_j, 0} F_{\{1-s_i\}_{i=1}^n, \{1-t_i\}_{i=1}^{j-1}, 0, \{1-t_i\}_{i=j+1}^n}^{(N-n+1-k)} \frac{\sqrt{\tilde{x}_j \gamma_{k+\sum_{j=1}^n t_j}}}{C_{\{1-s_i\}_{i=1}^j, 0, \{1-s_i\}_{i=j+1}^n, \{1-t_i\}_{i_1}^n}^{(N-n+1-k)}} \\ &+ (N-k-n+1) F_{\{1-s_i\}_{i=1}^n, \{1-t_i\}_{i_1}^n}^{(N-k-n)} \frac{\sqrt{\gamma_{k+s_1+s_2} \gamma_{k+t_1+t_2}}}{C_{\{1-s_i\}_{i=1}^n, \{1-t_i\}_{i_1}^n}^{(N-k-n)}} \end{aligned} \quad (33)$$

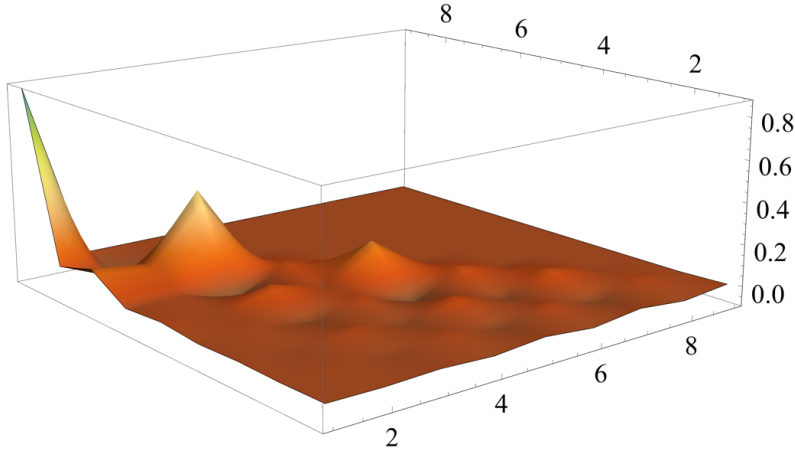


FIG. 12. Coefficients of the three-mode approximation of a superradiant state for $N = 8$ and $D = 8$.

with $k = 1, \dots, N - n$ and

$$F_{0,\dots,0}^{(0)} = 1, \quad (34)$$

and

$$c_{1-s_1, 1-s_2, 1-t_1, 1-t_2}^{(N-k-n+1)} = \sum_{i=1}^n s_i \left(\frac{x_i}{2} + i y_i \right) + t_i \left(\frac{\tilde{x}_i}{2} - i \tilde{y}_i \right) + \frac{1}{2} (\gamma_{\sum_{i=1}^n s_i + k} + \gamma_{\sum_{i=1}^n t_i + k}) + i(\omega_{k+\sum_{i=1}^n t_i} - \omega_{k+\sum_{i=1}^n s_i}). \quad (35)$$

This recurrence relation (33) can be computed through a matrix multiplication of $M^{\mathcal{O}(N)}$ in analogy with the previous sections, where M is now a matrix of size $(2^{2n}(N-n+1))^2$. Hence we notice that the complexity of the calculation grows exponentially with the order of the correlator.

E. Overlap

Consider the computation of $\langle 0 | c_1^{k_1} c_2^{k_2} \dots c_d^{k_d} | \phi^{(N)} \rangle$ with $\sum_{i=1}^d k_i = N$. This can be expressed by a linear combination of products of the form

$$\langle 0 | b_{x_1}^{k_1} b_{x_2}^{k_2} \dots b_{x_D}^{k_D} | \phi^{(N)} \rangle = \int_0^\infty \dots \int_0^\infty \left(\prod_{j=1}^N dt_j \right) \left(\prod_{j=1}^{k_1} B_{t_j}^{(x_1)*} \right) \left(\prod_{j=k_1+1}^{k_1+k_2} B_{t_j}^{(x_2)*} \right) \dots \left(\prod_{j=N-k_D+1}^N B_{t_j}^{(x_D)*} \right) A_{t_1 \dots t_N} \quad (36)$$

where we used (16). As in the previous section, we can compute each integral by solving the following recurrence relation:

$$F_{\{k_i - s_i\}_{i=1}^D} = \sum_{j=1}^D \theta[k_j - s_j] (k_j - s_j) F_{\{k_i - s_i\}_{i=1}^{j-1}, k_j - s_j - 1, \{k_i - s_i\}_{i=j+1}^D} \frac{\sqrt{x_j \gamma_{\sum_k s_k}}}{c_{\{k_i - s_i\}_{i=1}^{j-1}, k_j - s_j - 1, \{k_i - s_i\}_{i=j+1}^D}} \quad (37)$$

where $\theta[x]$ is the step function ($\theta[-|x|] = 0$ and $\theta[|x|] = 1$), together with the initial condition

$$F_{\{0\}_{j=1}^D} = 1, \quad (38)$$

and the coefficients

$$c_{\{k_i - s_i\}_{i=1}^D} = \frac{1}{2} \left(\sum_{j=1}^D s_j x_j + \gamma_{\sum_j s_j} \right). \quad (39)$$

This provides the desired solution as:

$$F_{\{k_i\}_{i=1}^D} = \langle 0 | b_{x_1}^{k_1} b_{x_2}^{k_2} \dots b_{x_D}^{k_D} | \phi^{(N)} \rangle \quad (40)$$

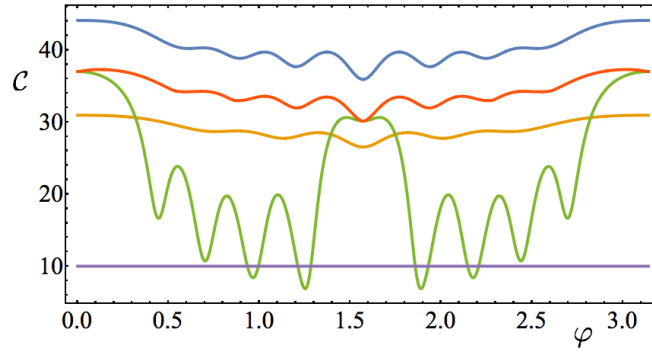


FIG. 13. Classical Fisher information in the presence of photon loss ($\eta = 0.95$) for: NR measurements in twin Fock states of $N = 8$ (orange) and $N = 10$ (blue) photons, and twin superradiant states with $N = 10$ and NR (green) and NMR (red) measurements. Finally, the straight purple line shows the classical Shot Noise Limit (SNL) corresponding to $C = N$.

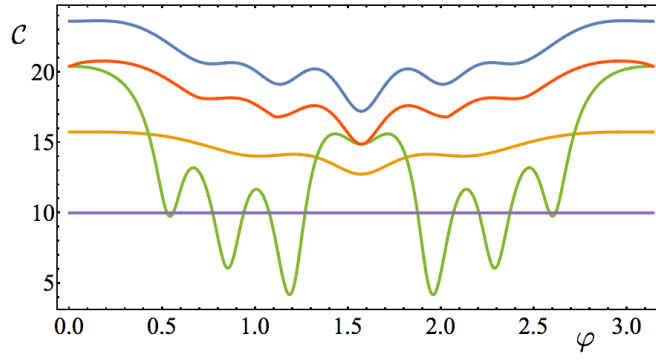


FIG. 14. Classical Fisher information in the presence of photon loss ($\eta = 0.9$) for: NR measurements in twin Fock states of $N = 6$ (orange) and $N = 8$ (blue) photons, and twin superradiant states with $N = 8$ and NR (green) and NMR (red) measurements.

Following the same logic as in the following sections, this integral can be computed by a product of matrices in a space of dimension

$$\dim = \prod_{j=1}^D k_j, \quad (41)$$

which is approximately bounded as

$$N \lesssim \dim \lesssim (N/D)^D. \quad (42)$$

In Figure 12 we illustrate these ideas by computing all $\langle 0 | c_1^{k_1} c_2^{k_2} c_3^{k_3} | \phi^{(N)} \rangle$ with $N = 8$, $D = 8$ and $d = 3$.

II. NUMERICAL RESULTS ON QUANTUM METROLOGY WITH PHOTON LOSS

This section shows more numerical results on the CFI with photon loss and considering as input states twin Fock states and twin superradiant states, as shown in Figures 13, 14 and 15.

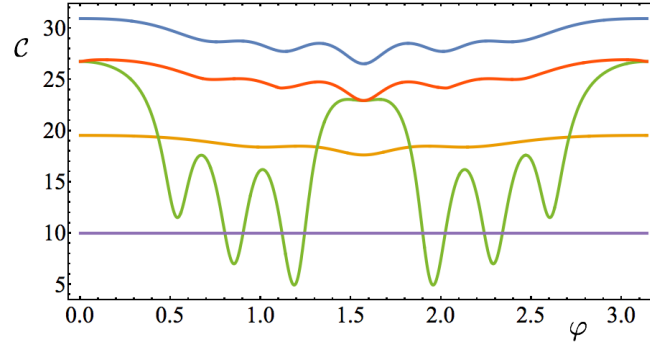


FIG. 15. Classical Fisher information in the presence of photon loss ($\eta = 0.95$) for: NR measurements in twin Fock states of $N = 8$ (orange) and $N = 10$ (blue) photons, and twin superradiant states with $N = 8$ and NR (green) and NMR (red) measurements.